

AD-A044 614

BATTELLE COLUMBUS LABS OHIO

F/G 11/6

IMPLICATIONS OF ALLOY STRUCTURE WITH RESPECT TO MECHANICAL PROP--ETC(U)

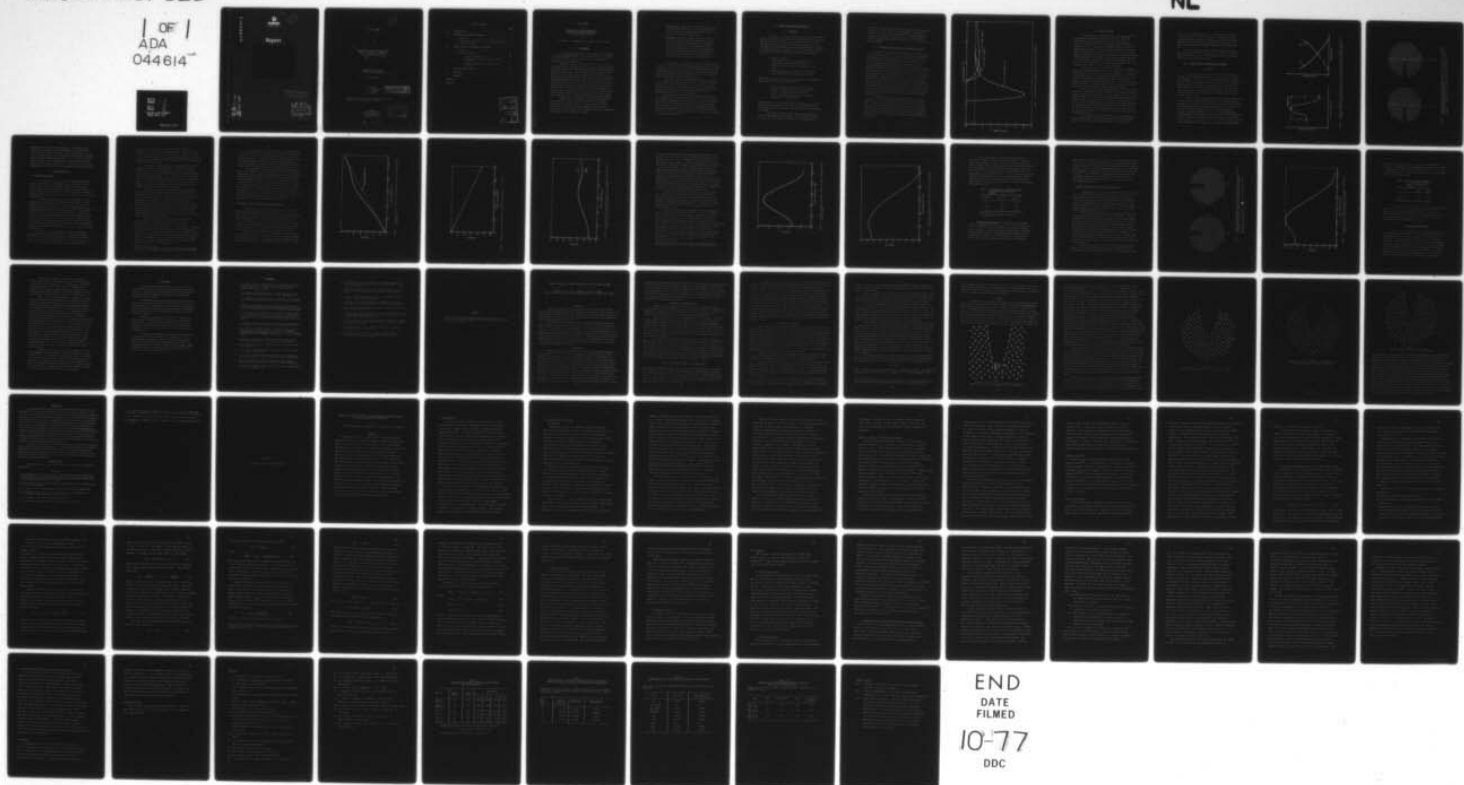
MAY 77 L R KAHN, A J MARKWORTH, P C GEHLEN

N00014-76-C-0181

NL

UNCLASSIFIED

1 OF 1  
ADA  
044614



END

DATE

FILMED

10-77

DDC

ADA044614



1  
12  
P.S.

# Report

DISTRIBUTION STATEMENT A  
Approved for public release  
Distribution Unlimited

AD No. 1  
FILE COPY

DD DC  
DRAFTED  
SEP 29 1977  
RELEASER  
A

(B)

Q  
FINAL REPORT.

on

Q  
IMPLICATIONS OF ALLOY STRUCTURE WITH  
RESPECT TO MECHANICAL PROPERTIES.

(Contract N00014-76-C-0181)

(15)

to

DEPARTMENT OF THE NAVY  
OFFICE OF NAVAL RESEARCH

Q 31 May 31, 1977

(B) 72p.

(10)

L. R./Kahn  
A. J./Markworth  
P. C./Gehlen  
G. T./Hahn

DISTRIBUTION STATEMENT A  
Approved for public release  
Distribution Unlimited

Reproduction in whole or in part is permitted for any  
purpose of the United States Government

BATTELLE  
Columbus Laboratories  
505 King Avenue  
Columbus, Ohio 43201

D D C  
REF ID: A  
SEP 23 1977  
REGULATORY  
A

H07080

AB

TABLE OF CONTENTS

	<u>Page</u>
I. INTRODUCTION . . . . .	1
II. HYDROGEN-ASSISTED CRACK PROPAGATION . . . . .	3
A. Background . . . . .	3
B. Interatomic Potentials for the Iron-Hydrogen System .	4
C. Simulation Studies . . . . .	6
III. EFFECTS OF LATTICE PERIODICITY ON FRACTURE . . . . .	7
A. Background . . . . .	7
B. Simulation Studies . . . . .	10
1. Computational Procedure . . . . .	10
2. Results - Effects of Variation of Stress Intensity . . . . .	12
3. Results - Effects due to Hydrogen at the Crack Tip . . . . .	20
IV. FLEXIBLE-BOUNDARY SCHEME . . . . .	23
V. CONCLUSIONS . . . . .	25
VI. REFERENCES . . . . .	26

APPENDIX A

APPENDIX B

ACCESSION NO.	
RTTB	White Section <input checked="" type="checkbox"/>
DTTB	Buff Section <input type="checkbox"/>
UNARMED	
CLASSIFICATION	
<i>Litter or file</i>	
BY	
DISPOSITION AVAILABILITY CODED	
DATE	AVAIL. AND OR SPECIAL
A	A

FINAL REPORT

on

IMPLICATIONS OF ALLOY STRUCTURE WITH  
RESPECT TO MECHANICAL PROPERTIES  
(Contract N00014-76-C-0181)

by

L. R. Kahn, A. J. Markworth, P. C. Gehlen, and G. T. Hahn

I. INTRODUCTION

The research described herein was carried out in fulfillment of Contract N00014-70-C-0390 and covers research carried out since the last major report<sup>(1)</sup> was issued. Publications written during this period are included as appendices.

The primary objective of this project has been to relate the toughness of metals, including effects of hydrogen, to physical properties at the atomic level. Our approach is based on computer-simulation techniques that describe a crack-containing crystal comprised of the order of a thousand atoms. With this approach (the details of which have been described elsewhere<sup>(2)</sup>), each atom is treated as a point mass, and appropriate pairwise central potentials are used to describe the interaction between any two atoms. The discrete atomic array is interfaced in such a manner with a surrounding continuum (see Section IV) that its behavior is characteristic of that of a corresponding array contained within a macroscopic crystal. In this manner, atomic arrangements can be simulated that are not amenable either to direct experimental observation or to treatment via closed-form analytical methods.

A number of basic problems were encountered in simulation studies carried out under a previous contract<sup>(1)</sup>. For example, calculations of the energy barrier to crack extension incorrectly predicted that the barrier failed to disappear at large levels of applied stress. These problems were ultimately traced to two fundamental shortcomings of the computational procedure:

Energy Exchange. The procedure failed to account for the energy exchanged between the continuum and the discrete atomic array. This basically was the reason for the anomalous behavior of the energy barrier.

Disregistry. We had not avoided small disregistries, of the order of the atomic spacing, between the crack-tip position implied by the continuum and that assigned by the discrete atomic array. The associated errors in energy calculations could be comparable in magnitude to the energy-exchange discrepancy, but of opposite sign. In some cases the two errors canceled. When they failed to cancel, they were attributed to the wrong source.

We were thus led to believe that a small rigid-boundary model could not be used to obtain physically meaningful results; efforts were consequently applied to the more complex flexible-boundary model, which contained the same flaw but for which its diagnosis was more difficult. During the present reporting period, methods for accounting for energy exchange and avoiding disregistry were developed.

Some other basic questions regarding our model still exist, e.g., concerning the manner in which atoms in the boundary contribute to the overall energy of the discrete region. However, we are now confident that the model as presently constructed, and upon which the results presented below are based, constitutes a useful tool for approximating the behavior of a "real" material.

> During this reporting period, research was carried out in the following areas: (1) construction of a physically realistic model for the atomic arrangement around a crack tip, as well as the development of "flexible boundaries"; (2) selection of an Fe-H interatomic potential together with its application to the simulation of hydrogen-assisted crack propagation; and (3) analysis of the effects of lattice periodicity on fracture, including effects due to the presence of hydrogen. The results are presented below.

## II. HYDROGEN-ASSISTED CRACK PROPAGATION

### A. Background

The presence of certain foreign species (e.g., sodium, helium, hydrogen, etc.) within materials can result in effects such as embrittlement, stress-corrosion cracking, and corrosion fatigue, which are immensely important. One aspect of this very broad subject that was considered in this program was hydrogen-induced embrittlement. Actually, as has been pointed out by Louthan et al.<sup>(3)</sup>, hydrogen embrittlement can result from a number of processes, including the following:

1. Hydride formation
2. Reaction between hydrogen and some impurity or alloy addition contained within the metal
3. Adsorption of hydrogen onto or absorption into the metal
4. Hydrogen "blistering" or cracking (resulting from hydrogen-gas build-up at microcracks and voids).

Mechanisms proposed to explain hydrogen embrittlement via adsorption and/or absorption include the following<sup>(3)</sup>:

1. Lowering of surface energy by hydrogen adsorption
2. Decrease of binding energy resulting from interaction of hydrogen with d-shell electrons
3. Buildup of internal gas pressure due to hydrogen precipitation at internal voids.

Absorbed hydrogen can also interact with dislocations (e.g., acting to pin dislocations or leading to the formation of gas-filled voids or microcracks at dislocation pileups) and can contribute to embrittlement in this manner.

Our studies of hydrogen embrittlement were concerned with effects of adsorbed/absorbed hydrogen on crack propagation in  $\alpha$ -iron. No account was taken, however, of effects due to the presence of

hydrogen on the Fe-Fe interaction, so that possible contributions due to mechanism 2 were not included. Quantum-mechanical approaches are currently being used at Battelle-Columbus<sup>(4)</sup> to gain information of this nature. The present research was based on current knowledge regarding pairwise Fe-Fe and Fe-H interactions. The H-H interaction was not included.

#### B. Interatomic Potentials for the Iron-Hydrogen System

Simulation studies of hydrogen-assisted crack propagation in  $\alpha$ -iron were carried out as part of this research using a simple model, as described below. As far as the Fe-H interaction was concerned, initial studies<sup>(5)</sup> were based on data calculated by Walker et al.<sup>(6)</sup> for the FeH molecule using many-body perturbation theory. Later studies (summarized below and described in detail in Appendix A, and Reference (7)) were based on the Fe-H potential calculated by Olander<sup>(8)</sup> using experimentally determined data for hydrogen in iron, namely, the heat of solution, the heat of adsorption, and the activation energy for bulk diffusion. These potentials are presented in Figure 1 together with the Johnson Fe-Fe potential<sup>(9)</sup> that was used in the same analyses. It can be seen that the well depth for the Walker potential is about an order of magnitude greater than that for the Olander potential and also that the interatomic distance at which this depth occurs is much shorter for the former potential than for the latter. In addition, the Olander potential extends to significantly larger interatomic distances than the Walker potential.

It must be emphasized that the Fe-H potential is of great importance in this type of study and must be known with more certainty than is presently available before more confidence can be had in the results of the simulations. Nevertheless, the significant differences between these two Fe-H potentials can be exploited in obtaining information regarding effects of variations in Fe-H interaction parameters (well depth, etc.) on overall crack-tip behavior under the influence of applied stress.

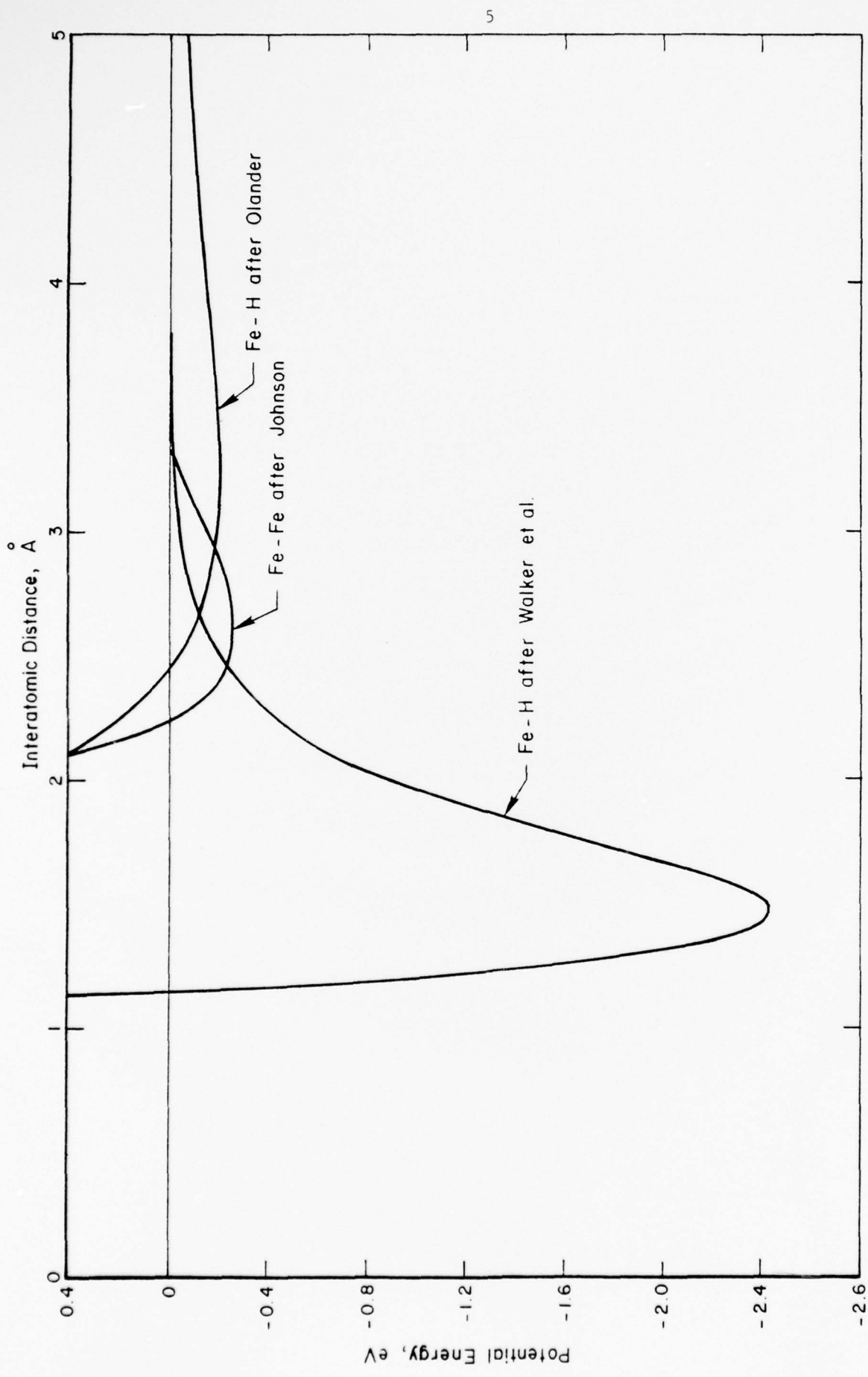


FIGURE 1. ILLUSTRATION OF INTERATOMIC POTENTIALS USED IN THIS RESEARCH

### C. Simulation Studies

For our analyses of hydrogen-assisted crack propagation<sup>(5,7)</sup>, a two-dimensional crack model for  $\alpha$ -iron was used, the crack "tip" actually being an infinitely long "line". Our results were found to vary only slightly with the type of boundary condition used, i.e., flexible or rigid. A single atom of hydrogen (actually, a "line" of hydrogen atoms parallel to the line defining the crack tip) was placed within the lattice near the crack tip in such a location that maximum effect on crack-tip behavior under the influence of applied stress would likely be observed. In this light, this system constitutes a model of a form of embrittlement resulting from "absorption" of hydrogen into the lattice. It is clear, however, that these studies represent only a first step toward the solution of a very complicated problem.

For the case (Reference 5) in which the Walker Fe-H potential was used, it was found that the effect of the hydrogen was to shorten the distances between the four iron atoms which surrounded it. Consequently, the Fe-Fe bonds beyond were elongated, and finally broke, one at a time, at a load about 10 percent smaller than the normal failure load for  $\alpha$ -iron. This behavior can be understood in terms of the form of the Fe-H potential function (see Figure 1) which exhibits a deep attractive well located at a relatively small interatomic separation (1.49A).

For the case in which the Olander potential was used (Appendix A, Reference 7), the results were quite different. The hydrogen was found to cause severe distortion of the lattice in its vicinity, the crack tip being markedly widened. The degree of crack-propagation enhancement was found, however, to be relatively insensitive to the level of applied stress, in contrast to the corresponding results obtained using the Walker potential. The distorting effect of the Olander potential can be attributed to the fact that it becomes repulsive at relatively large interatomic separations (see Figure 1), the effect of the hydrogen thus being to "push away" the surrounding iron atoms.

It is interesting to observe that both the Fe-H potentials did result in effects which could be interpreted as forms of embrittlement despite the fact that the potentials themselves had quite different

properties, as illustrated in Figure 1. We are thus led to the conclusion that the Fe-H interaction, as well as changes in the Fe-Fe interaction due to the presence of hydrogen, must be known with significantly greater precision before more definitive conclusions can be drawn regarding mechanisms of hydrogen embrittlement at the atomistic level.

The hydrogen-embrittlement problem is examined from another point of view in Section III. Analyzed there are effects of hydrogen, situated at the tip of a crack, on the energetics of crack propagation through the discrete crystalline lattice.

### III. EFFECTS OF LATTICE PERIODICITY ON FRACTURE

#### A. Background

For a crack-propagation theory based purely on continuum mechanics, energy changes associated with crack extension (or healing) are independent of the structure of the crystalline lattice. However, since a "real" solid exhibits atomic-level periodicity, one would consequently expect periodic effects, on the atomic scale, associated with crack propagation. Such effects are well known, of course, for other types of defects, such as dislocations and vacancies, and indeed have also been described in terms of effects on fracture (as, for example, in References 10 to 18).

Interest in lattice-periodicity effects results principally from the fact that, for a range of stress intensities, an activation-energy "barrier" must be overcome in order to extend or close a crack by a single lattice-repeat distance, as illustrated in Figure 2a. The magnitudes of such barriers would be dependent upon the stress-intensity level as shown schematically in Figure 2b. Two successive minimum-energy configurations are illustrated in Figure 3 for a crack tip in a model bcc crystal. The crack-tip separation for these two cases is one-half the lattice parameter. It is apparent that crack extension can thus take place, from one equilibrium site to another, as a thermally activated process,

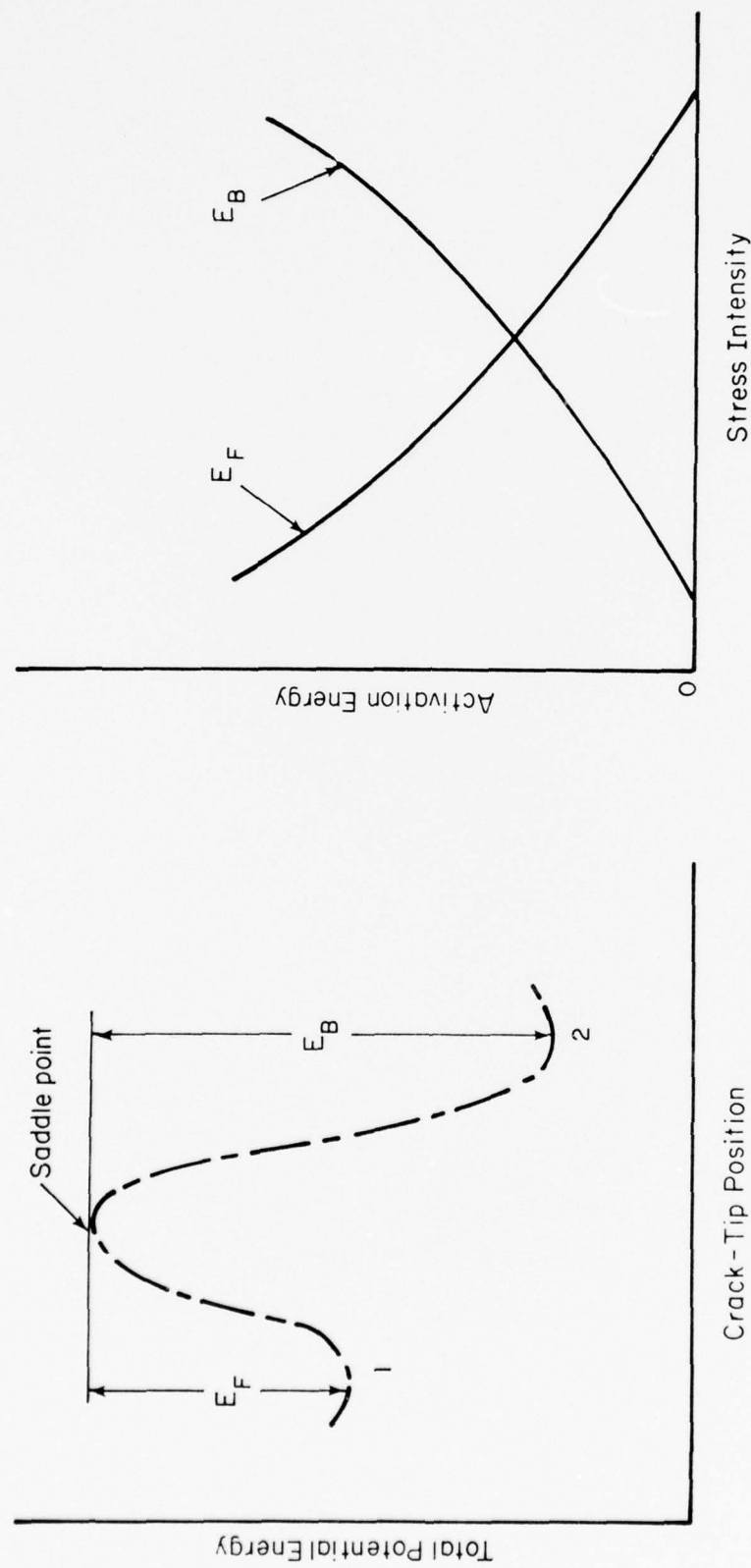


FIGURE 2. SCHEMATIC ILLUSTRATION OF THE VARIATION OF (a) THE CRYSTALLINE POTENTIAL ENERGY WITH CRACK-TIP POSITION, AND (b) THE MAGNITUDE OF THE ACTIVATION-ENERGY BARRIERS WITH STRESS INTENSITY

(b)

(a)

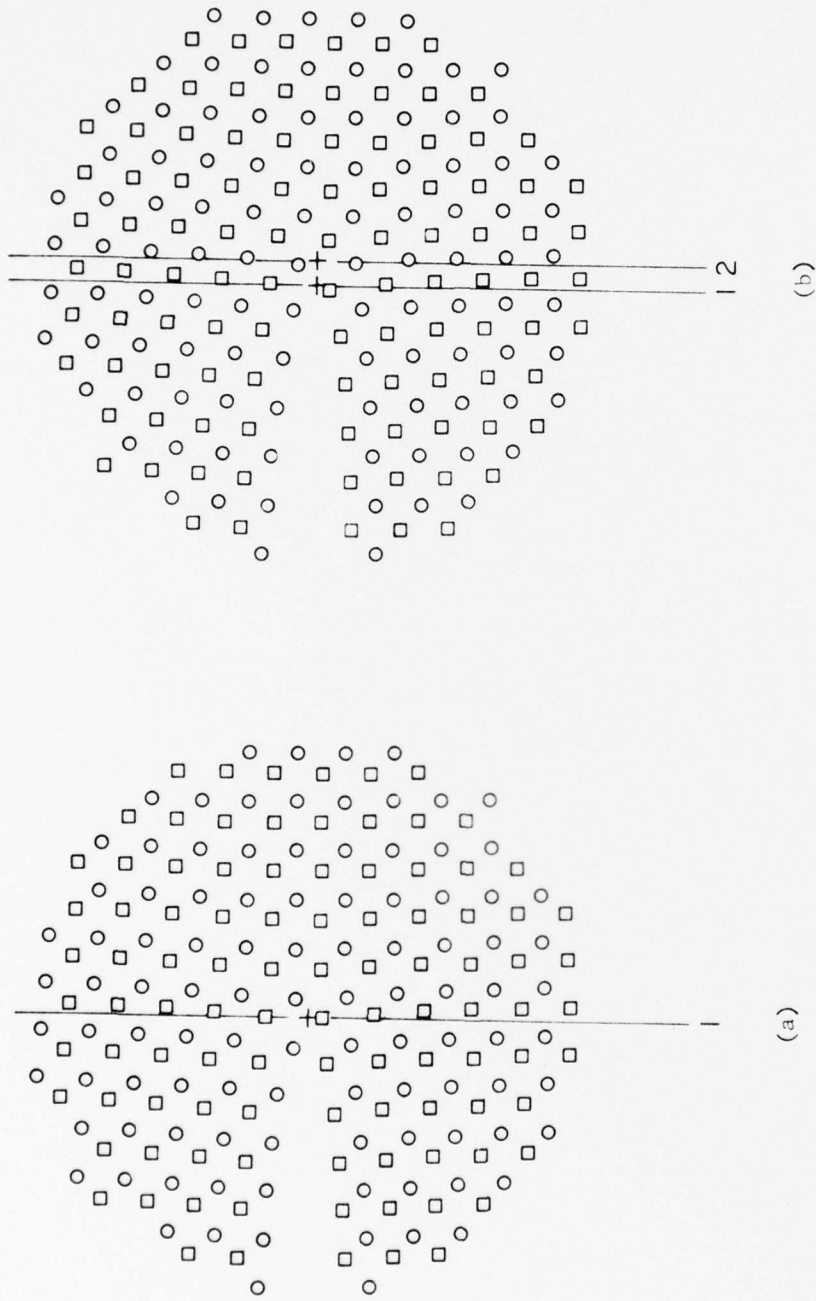


FIGURE 3. ILLUSTRATION OF THE ATOMIC CONFIGURATIONS AROUND A CRACK TIP ( $K = 0.2 \text{ eV}/\text{\AA}^{5/2}$ ) FOR TWO DIFFERENT CRACK-TIP POSITIONS: (a) crack-tip located at Position 1; (b) crack tip located at Position 2, one-half lattice parameter beyond Position 1. These are successive minimum-energy configurations.

analogous to other types of defect migration. Also, herein lies an additional possible mechanism for embrittlement by a foreign atomic species, namely, through the action of such a species (a) to reduce the activation-energy barrier for crack extension and thus permit the crack to advance at lower stress-intensity levels, and (b) to enhance thermally-induced extension. This could take place by effects that the foreign species has on metal-metal bonds and/or by alterations produced in atomic arrangements at the crack tip due to the presence of the foreign species.

### B. Simulation Studies

#### 1. Computational Procedure

Our simulation studies of effects of lattice periodicity on fracture were based on a two-dimensional crack model similar to that used to simulate hydrogen-embrittlement effects (see Section IIC). However, as indicated above, additional complications were involved in the lattice-periodicity studies due to disregistry and energy-exchange problems as well as to problems involved with determination of saddle-point configurations.

A relatively simple model was found to be adequate for these computations; it consisted of 165 movable atoms surrounded by a rigid boundary. Within the boundary, the atomic positions were taken, for any given location of the crack tip, to be in accordance with the displacement field predicted by linear-elastic theory<sup>(19)</sup>. The potential energy of the atomic array was determined as a function of crack-tip position by reducing the discrete configuration to its minimum potential energy for various locations of the crack tip along a <100> direction. The relaxation procedure was carried out using the "kinetic-energy quench" method described elsewhere<sup>(2)</sup>. (We note, however, that other appropriate minimization techniques could, in principle, be used to find minimum-energy configurations.)

The energy of the entire crystalline system was estimated, for any given crack-tip position, by adding to the potential energy of the relaxed discrete region the appropriate contribution of the linear-elastic region, that being  $\gamma b (K_b/K_G)^2$  where K is the stress intensity,  $\gamma$  and b are, respectively, the surface energy and lattice parameter of

the iron crystal,  $K_G$  is the stress intensity at the Griffith level (numerical values for  $\gamma$ ,  $b$ , and  $K_G$  being  $0.081\text{eV}/\text{\AA}^2$ ,  $2.86 \text{\AA}$ , and  $0.242 \text{eV}/\text{\AA}^{5/2}$ , respectively), and  $f$  is a unitless parameter equal to the number of half lattice-parameters the crack tip has been moved relative to some arbitrarily chosen reference position ( $f$  being positive for crack healing, negative for crack extension).

The atomic configurations which were sought were those which exhibited a minimum in potential energy as a function of crack-tip position, since it was these configurations for which no disregistry existed between the crack-tip position implied by the continuum and that assigned by the discrete atomic array. The nature of these minima was found to be dependent upon stress intensity, that is, an energy minimum might exist either for the discrete region or for the total system (discrete region plus continuum) depending upon the magnitude of the  $K$ -level. This effect was an artifact of the model.

As expected, adjacent minima obtained through this procedure were found to be characterized by crack-tip positions separated by about  $b/2$ , which is the lattice repeat distance along a  $<100>$  direction for this crack configuration. In other words, periodic variations of energy associated with the crack exhibited the periodicity of the lattice itself. Deviations from this behavior could exist, however, if the lattice were to be disturbed in some manner, such as by the presence of a foreign species (as was indeed found for the situation described below in which hydrogen was placed near the crack tip). It was the atomic configurations at adjacent minima that were of concern in subsequent calculations, as now described.

Potential-energy values for the atomic array, at given positions along a vector in configuration-space\* joining two adjacent minima, were estimated by using a procedure in which each atom in the array and in the boundary was "marched" (i.e., displaced) by identical fractional amounts along the vector (in three-dimensional space) joining its positions at the two minima. The potential energy of the array was calculated at these various intermediate positions along the "march". The maximum energy thus calculated, at one of the intermediate positions, represented an estimate (actually, an overestimate) of the "saddle-point" energy of the discrete array.

---

\*For a given N-atom system, its vector in configuration space would consist of the set of  $3N$  position coordinates characterizing all the atoms.

Two points should be noted relative to the "march" procedure: (1) Only the two end-point configurations of atoms were "relaxed" (i.e., minimum-energy) configurations. (2) One can show that, in the linear-elastic approximation, the fraction which describes the degree to which the atoms are displaced between the end points equals the fraction describing the degree to which the crack-tip (as defined by the linear-elastic field) is displaced between its two end-point positions.

Our saddle-point calculation was carried out using an approach based on the technique of Sinclair and Fletcher<sup>(20)</sup>, the latter having been adapted from the conjugate-gradients method for function minimization developed earlier by Fletcher and Reeves<sup>(21)</sup>. The Sinclair-Fletcher method is designed to locate equilibrium configurations characterized by one unstable mode of vibration. Two attractive features of the method are: (1) Its success does not depend on constraints placed upon any of the coordinates or upon symmetry within the structure. (2) First (not second) derivatives of the objective function are required. For our applications, the initial estimate used for the saddle-point location was the atomic configuration corresponding to the maximum energy of the discrete array calculated using the "march" procedure.

## 2. Results - Effects of Variation of Stress Intensity

Computations were carried out, using the procedures described above, for three different levels of stress intensity:  $K = 0.2, 0.242,$  and  $0.4 \text{ eV}/\text{\AA}^{5/2}$ , the second of the three values being the stress-intensity level  $K_G$  predicted from the Griffith theory. One would expect, on the basis of continuum theory alone, that crack extension would occur for  $K > K_G$ , and crack healing for  $K < K_G$ . Our goal, in carrying out these computations, was to determine the height of activation-energy barriers for both crack opening and closure as the crack tip was moved along a straight line from one given minimum-energy position to the next.

Results for  $K = 0.2 \text{ eV}/\text{\AA}^{5/2}$  are presented in Figures 4 through 6, the atomic configurations corresponding to the two calculated minimum-energy configurations (i.e., at crack-tip locations 0 and  $b/2$ ) being in fact those shown in Figure 3. In particular, shown in Figure 4, is the

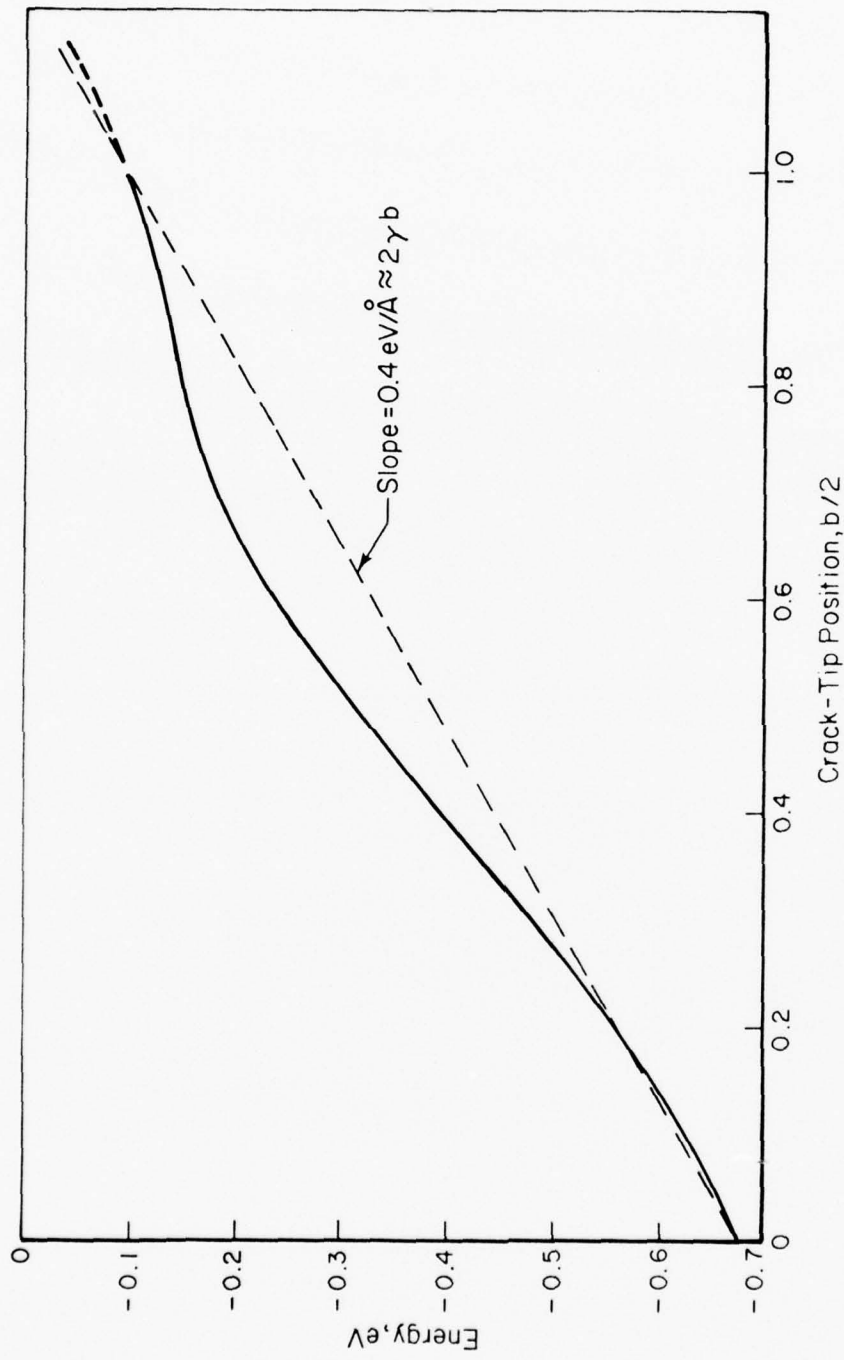


FIGURE 4. VARIATION OF POTENTIAL ENERGY OF DISCRETE REGION WITH CRACK-TIP POSITION FOR  
 $K = 0.2 \text{ eV}/\text{\AA}^2$ .

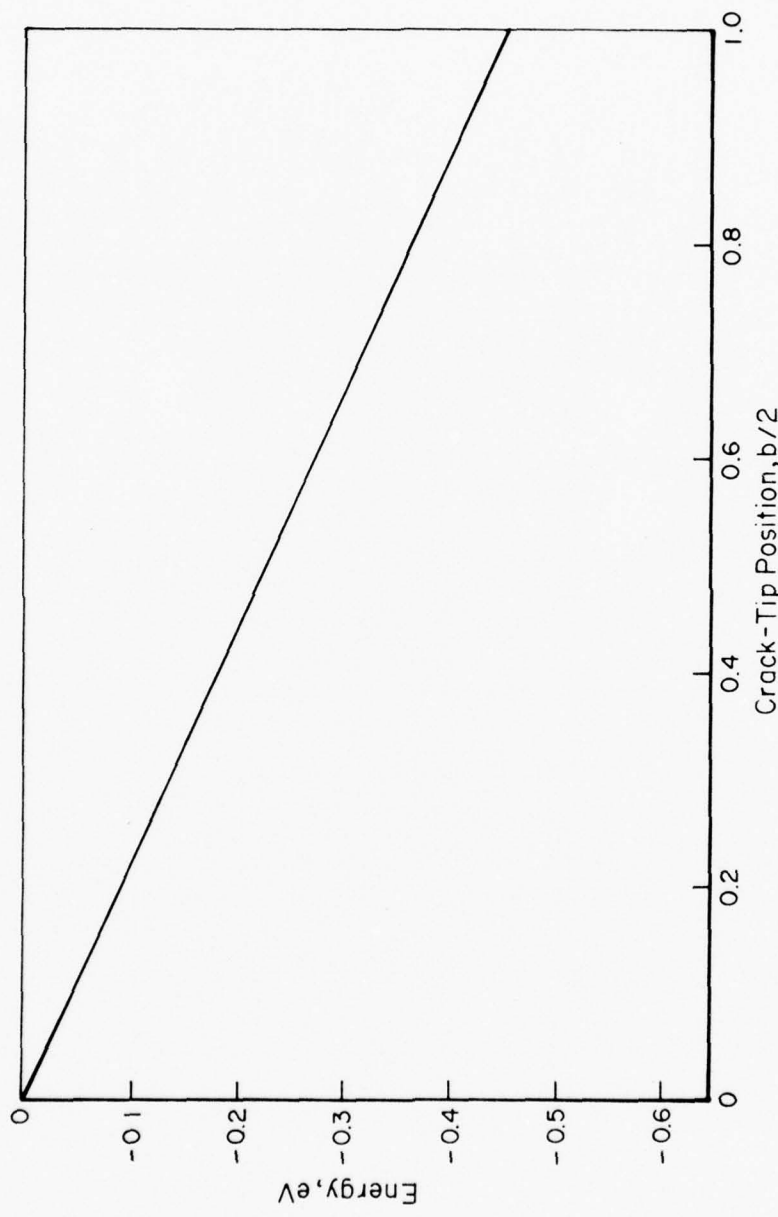


FIGURE 5. VARIATION OF CONTINUUM ENERGY WITH CRACK-TIP POSITION FOR  $K = 0.2 \text{ eV}/\text{\AA}^{5/2}$ .

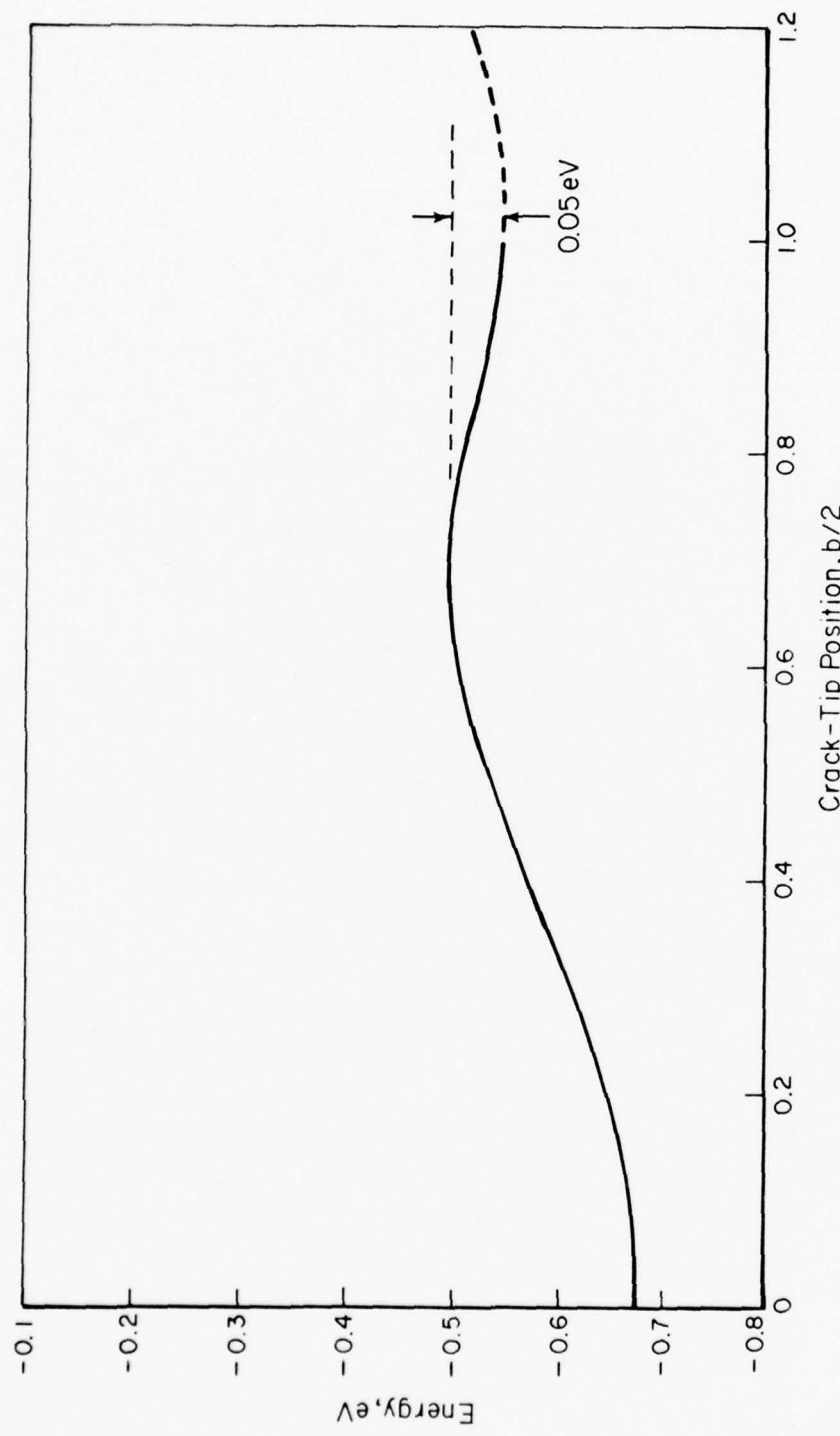


FIGURE 6. VARIATION OF TOTAL CRYSTALLINE ENERGY (THAT OF DISCRETE REGION PLUS THAT OF CONTINUUM) WITH CRACK-TIP POSITION FOR  $K = 0.2 \text{ eV}/\text{\AA}^{5/2}$ .

variation of potential energy\* of the atomistic region with crack-tip position, in Figure 5 is that of the continuum, and in Figure 6 is that for the entire crystal (i.e., the sum of the two). For purposes of comparison, all three figures are drawn to the same scale of both energy and crack-tip displacement. A number of points should be noted: First, it can be seen from Figure 4 that the minimum-energy points are now shifted away somewhat from the end-point (and relaxed) configurations. Second, the average energy increase associated with the crystallite in extending the crack between adjacent minima is about equal to the concomitant increase of surface energy, indicating that the model is well-behaved. Third, we observe, from Figure 6, that energy barriers to both opening and closure do indeed exist. Of course, there is a net increase of energy as the crack tip advances from one minimum-energy configuration to the next, since the  $K$  level is below the Griffith value.

Thus, despite the fact that, at this  $K$  level, crack closure would, on the basis of continuum theory, be energetically favored to occur at any crack-tip position, the present model exhibits an energy barrier to closure of about 0.05 eV. Accordingly, crack healing can be regarded as a thermally activated process, with a "characteristic temperature" being defined as  $E/k \approx 300^\circ\text{C}$  where  $E$  is the barrier height and  $k$  the Boltzmann constant.

Results analogous to those presented in Figure 6 are shown in Figures 7 and 8 for  $K = 0.242$  and  $0.4 \text{ eV}/\text{\AA}^{5/2}$ , the former corresponding to the Griffith value. For both situations, energy barriers to both crack opening and closure exist. At the Griffith level, little net energy change exists between adjacent minima, as expected. Also, for  $K = 0.4 \text{ eV}/\text{\AA}^{5/2}$ , the net energy at successive minima decreases as the crack tip advances, also as expected. The fact that the energy minima calculated at the Griffith level are not at the same value of energy can be attributed largely to approximations inherent in the model. For example, some portion of the elastic energy attributed to the continuum was contained within the discrete region and was thus also included in the potential energy calculated for that region.

---

\*Absolute energies are unimportant for present considerations, and only energy changes relative to crack-tip position have significance here.

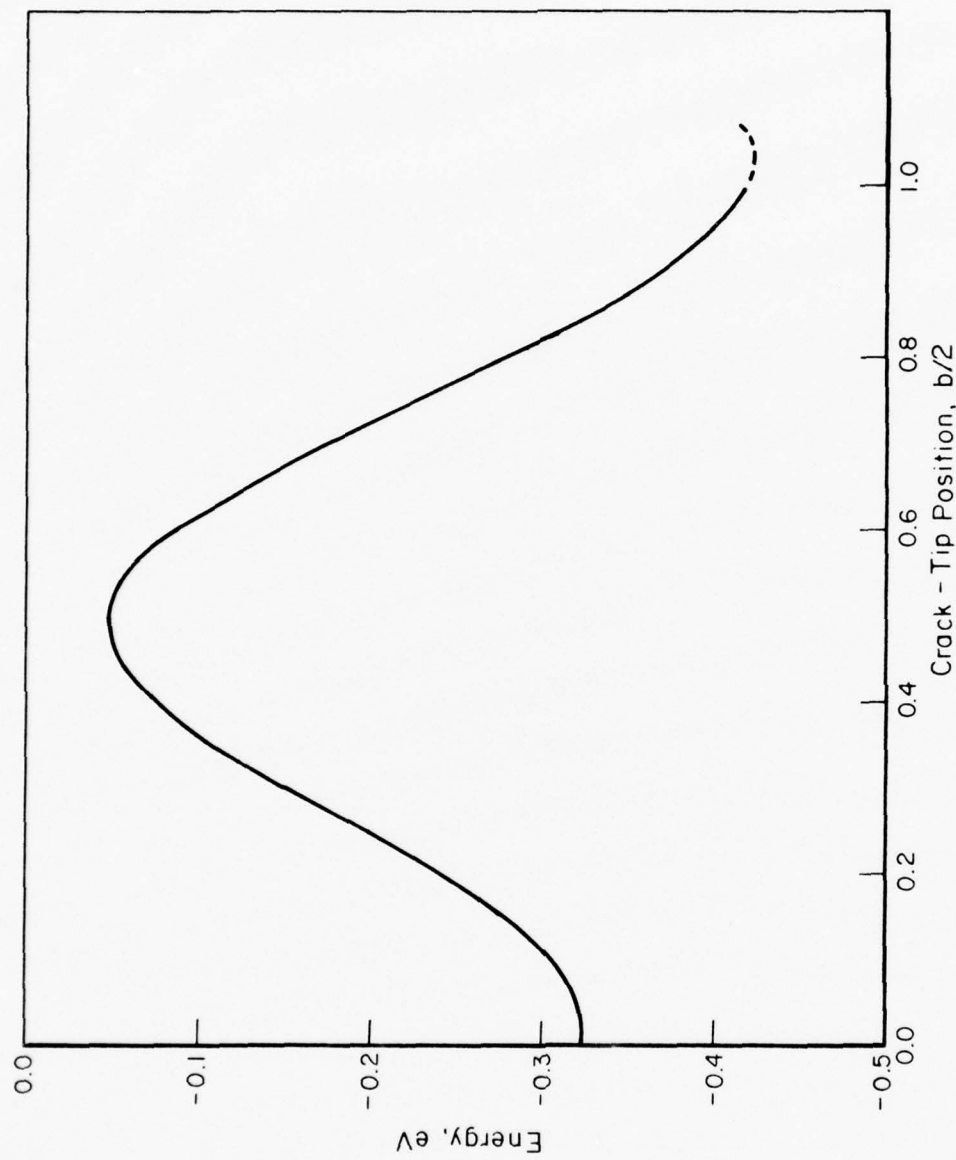


FIGURE 7. VARIATION OF TOTAL CRYSTALLINE ENERGY WITH CRACK-TIP POSITION FOR  
 $K = 0.242 \text{ eV}/\text{\AA}^{5/2}$ .

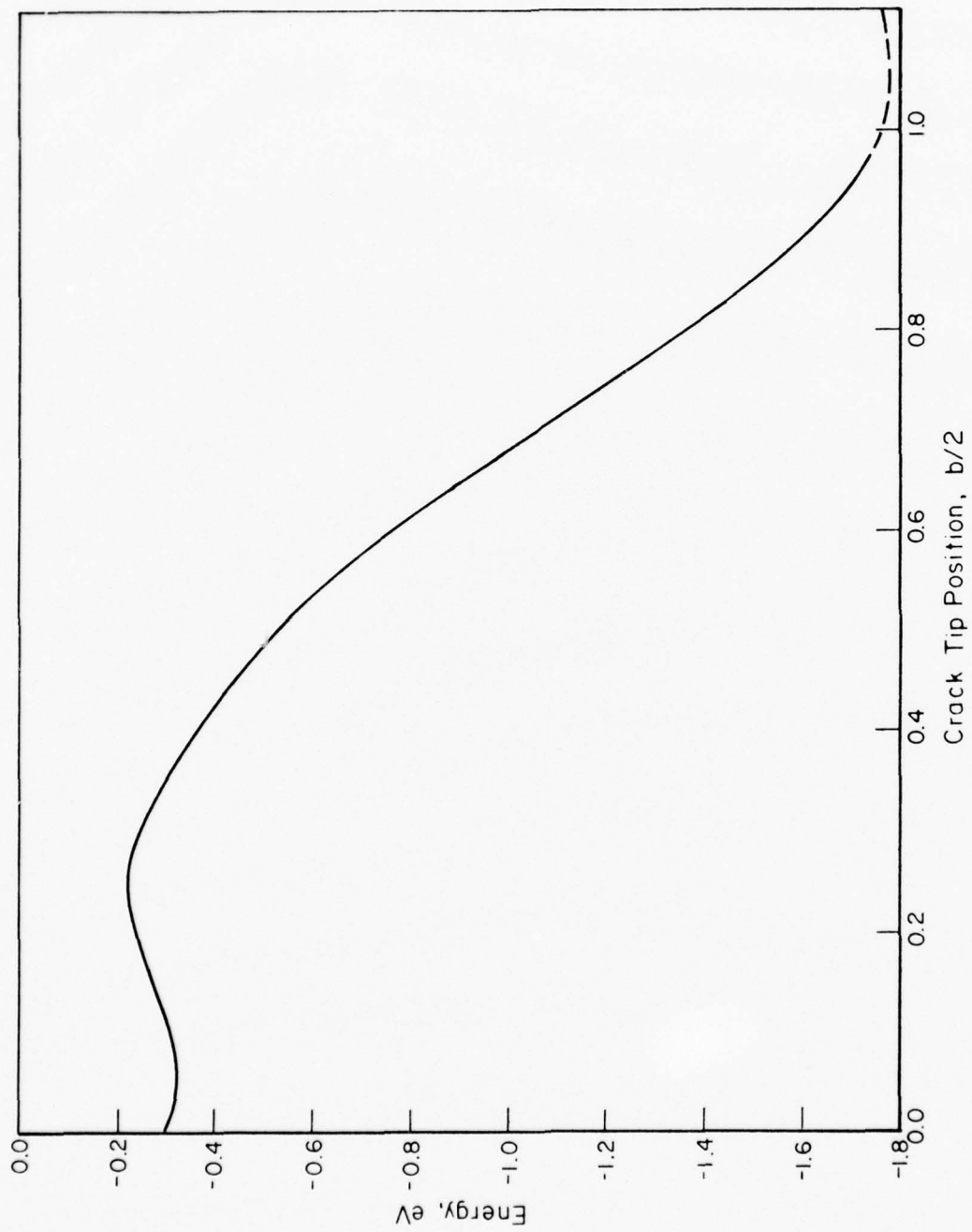


FIGURE 8. VARIATION OF TOTAL CRYSTALLINE ENERGY WITH CRACK-TIP POSITION  
FOR  $K = 0.4 \text{ eV}/\text{\AA}^{5/2}$ .

The activation-energy barriers calculated from results illustrated in Figures 6 through 8 are listed in Table I. The barrier  $E_B$  for backward movement is seen to increase rapidly with increasing K-level, whereas that for forward motion decreases with increasing K-level, albeit more slowly, and exhibits some fluctuating behavior ( $E_F$  for the  $K = 0.2 \text{ eV}/\text{\AA}^{5/2}$  being greater than that for  $0.242 \text{ eV}/\text{\AA}^{5/2}$ ) due to the approximate nature of the model. Also, it should be emphasized that these calculations were based entirely on results obtained from the "march" procedure; no saddle-point computations were involved here, although results obtained using the Sinclair-Fletcher<sup>(20)</sup> procedure were obtained and are described below.

TABLE I. ACTIVATION-ENERGY BARRIERS CALCULATED FOR FORWARD AND BACKWARD CRACK MOVEMENT

$K(\text{eV}/\text{\AA}^{5/2})$	$E_F(\text{eV})$ (a)	$E_B(\text{eV})$ (a)
0.2	0.18	0.05
0.242	0.27	0.37
0.4	0.10	1.54

(a) The energies  $E_F$  and  $E_B$  are defined in Figure 2a.

Saddle-Point Determination. The saddle-point configuration could not be determined for one of the three cases studied, namely, that for  $K = 0.2 \text{ eV}/\text{\AA}^{5/2}$  since the crystallite did not exhibit a maximum-energy configuration at some point between adjacent minima. (A maximum was found, however, when the continuum-energy contribution was added, as illustrated in Figure 4, so that the absence of a maximum for the discrete region alone was simply an artifact of the present model.)

Nevertheless, to illustrate the procedure, the saddle-point configurations for the other two K-levels were determined. Our method was based on the Sinclair-Fletcher<sup>(20)</sup> technique, and included modification of the crack-tip position at various places in the saddle-point search. It was thus found that the saddle point energies for the discrete region for  $K = 0.242$  and  $0.4 \text{ eV}/\text{\AA}^{5/2}$  were, respectively, only about 0.02 and 0.06 eV below the corresponding energy maxima determined from the "march" procedure, so that these maxima did represent relatively good approximations to the actual saddle-point energies.

### 3. Results - Effects due to Hydrogen at the Crack Tip

The computation of energy versus crack-tip position was repeated for  $K = 0.242 \text{ eV}/\text{\AA}^{5/2}$  but with hydrogen present at the crack tip in a manner analogous to that in an earlier study (Reference 7, Appendix A). The purpose of this work was to determine the effect of the presence of hydrogen on the magnitudes of the activation-energy barriers for crack extension and healing, and thus to assess whether or not the calculated alterations due to hydrogen would result in effects that could be interpreted as embrittlement of the metal.

For these computations, the Olander Fe-H potential<sup>(8)</sup> was used, in a manner analogous to that employed in previous work<sup>(7)</sup>. The atomic configurations around the crack tip corresponding to two adjacent minima in the potential energy of the entire system (discrete region, including the Fe-H and Fe-Fe energy, plus continuum) are illustrated in Figure 9. These minima were separated by slightly more than one lattice parameter, in contrast with all the analogous computations without hydrogen for which the minima were separated by only about half a lattice parameter, an effect brought about by the presence of hydrogen. Also, the total energy of the hydrogen-containing system was found to be several eV less than characterizing the same system, at the same K-level, but without the "line" of hydrogen atoms.

Results of carrying out the "march" procedure are presented in Figure 10, and the associated barrier heights are listed in Table II together with the corresponding energies for the iron system at the same

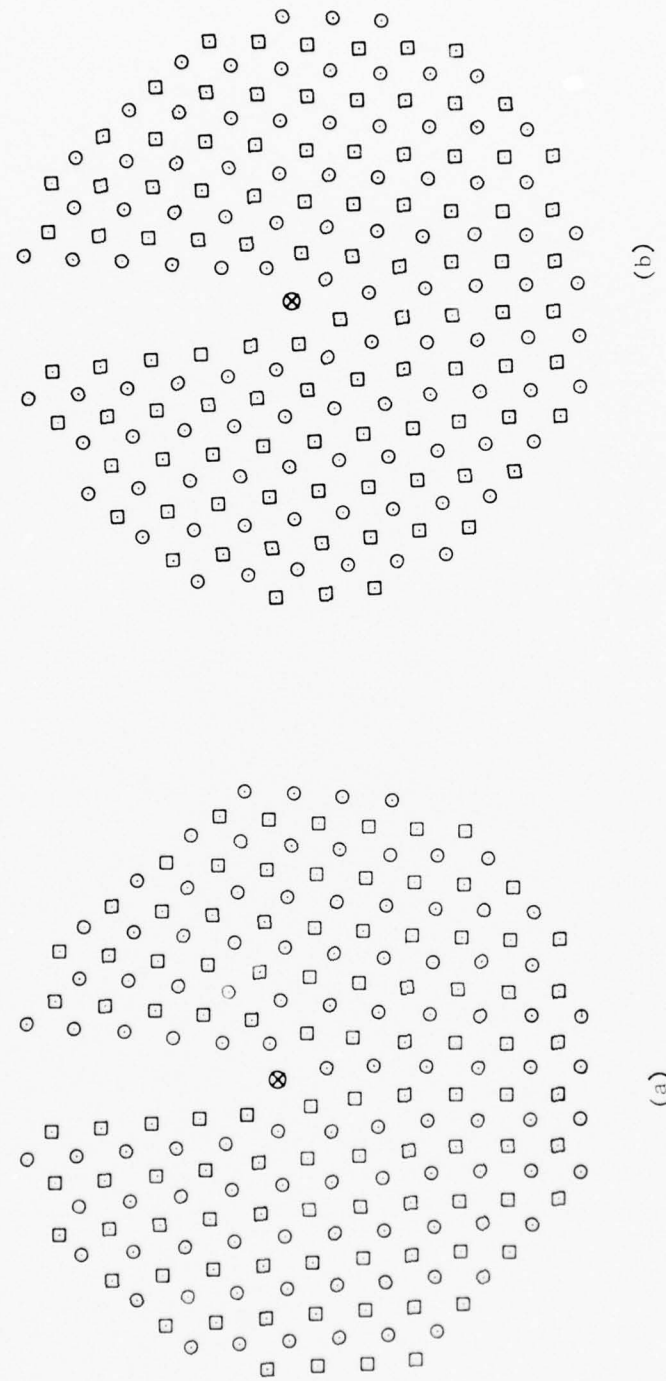


FIGURE 9. ATOMIC CONFIGURATIONS AROUND A HYDROGEN-CONTAINING CRACK ( $K = 0.242 \text{ ev}/\text{\AA}^{5/2}$ ) CORRESPONDING TO ADJACENT MINIMA IN THE TOTAL CRYSTALLINE ENERGY.

The hydrogen atom is denoted by  $\otimes$ , and the crack-tip at (b) is advanced by 1.1b beyond that at (a).

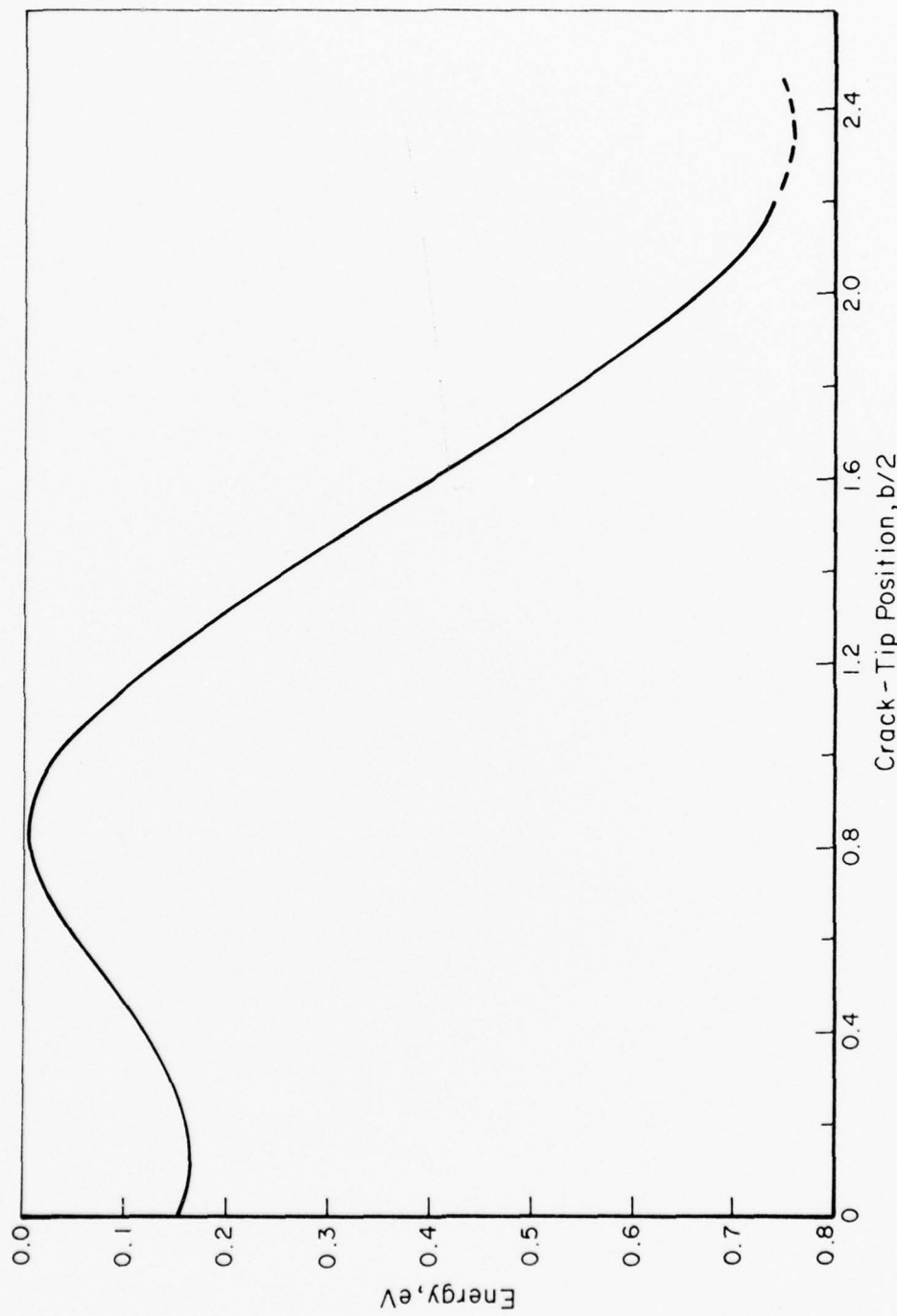


FIGURE 10. VARIATION OF TOTAL CRYSTALLINE ENERGY WITH CRACK-TIP POSITION FOR HYDROGEN-CONTAINING CRACK ILLUSTRATED IN FIGURE 9.

K-level but without hydrogen. It can be seen that the effect of the hydrogen is to decrease  $E_F$  and to increase  $E_B$ . Consequently, the crack is energetically easier to open and more difficult to close as a result of the hydrogen, factors which are consistent with the view of hydrogen acting as an embrittling agent.

TABLE II. ACTIVATION-ENERGY BARRIERS AT  
 $K = 0.242 \text{ eV}/\text{\AA}^{5/2}$  WITH AND  
 WITHOUT THE PRESENCE OF  
 HYDROGEN

	$E_F$ (eV)	$E_B$ (eV)
No Hydrogen	0.27	0.37
With Hydrogen	0.16	0.75

It should be noted that the specific results obtained here are peculiar to this particular configuration of hydrogen in iron. In general, calculated barrier heights are expected to depend upon such factors as the manner in which hydrogen is distributed along the crack-tip surface and within the volume of the iron around the crack tip. Additional research along these lines is needed.

#### IV. FLEXIBLE-BOUNDARY SCHEME

A problem of crucial importance in the atomistic simulation of crystal defects is the manner in which the discrete atomic array is interfaced with the surrounding continuum. The use of "flexible boundaries", in which atoms within the boundary are not held rigidly in place, but are allowed to relax to positions of lower potential energy, results in a number of benefits. Principally, the constraints imposed by "rigid" boundaries, which can lead to non-physical behavior (such as extraneous stress fields at the boundary), are removed. In addition, with flexible boundaries one can use a smaller array of atoms in the discrete region and thus improve the efficiency of the computation.

In this light, an updated form of Battelle's flexible-boundary scheme, "Flex-II", was developed as part of this program, and is described in detail in Appendix B (also Reference 22). The method basically consists of a set of steps, for most of which certain alternatives exist regarding detailed procedure. These steps are briefly summarized below in terms of a dislocation simulation, although the procedure is applicable to other types of line defects as well.

First, an array of atomic positions is generated for a region of perfect lattice, one crystallographic repeat distance thick in the direction along which the dislocation is to lie. Second, an initial dislocated configuration is generated by displacing all atoms according to a linear-elastic displacement field. The crystal is then divided into three regions: region I containing those atoms which behave in a substantially nonlinear manner and are thus relaxed independently; region II which surrounds region I and contains all atoms which lie within the range of interaction of at least one region-I atom; region III which surrounds region II and is comprised of that portion of the crystal which is necessary to fully define the force on each region-II atom. The following third and fourth steps are then repeated alternately: Third, the atoms in region I are relaxed toward equilibrium according to the atomic-force law. Precise equilibrium is not sought here, since later steps disturb the region by changing the boundary conditions. Fourth, the forces still remaining on the region-II atoms are used to generate a corrective displacement field for all three regions using Green-function techniques. The last two steps are repeated iteratively until no atoms in regions I or II have a resultant force greater than some selected tolerance.

The method thus devised was found<sup>(22)</sup> to be superior to earlier flexible-boundary schemes with respect to speed of computation. It was also found<sup>(22)</sup> that, in the analysis of core contributions to a dislocation strain field, nonlinear effects were fully allowed for without it being necessary to use a nonlinear elastic solution for the displacements. In addition, this approach resulted in calculation of the overall dilatation of a finite body due to a dislocation, with earlier conflicting calculations of this quantity having been corrected and reconciled.

## V. CONCLUSIONS

- Effects of hydrogen situated near the tip of a crack in  $\alpha$ -iron have been investigated using two widely differing Fe-H pairwise potentials. In both cases, the iron was "embrittled" as a result of the presence of hydrogen, although the mechanism for embrittlement was different for the two cases.
- Computational procedures have been developed with which the energy variations associated with crack propagation through a discrete crystalline lattice can be calculated. These were applied to studies of "lattice trapping" of cracks in  $\alpha$ -iron as a function of stress-intensity level, including calculation of activation-energy barriers for crack extension and healing.
- Effects of inclusion of hydrogen near the crack tip on lattice-trapping properties were also considered for a given stress-intensity level. It was found that hydrogen caused the activation-energy for crack extension to be reduced and that for crack healing to be increased, factors consistent with the concept of hydrogen acting to embrittle iron.
- A technique was developed for applying flexible boundaries to atomistic models of line defects, so that compatibility can be achieved between the discrete, atomistic region and the surrounding, outer region described in terms of continuum elastic solutions. The technique was found to be superior to earlier flexible-boundary schemes, with respect to speed of computation, and yielded satisfactory results relative to dislocation properties for  $\alpha$ -iron.

VI. REFERENCES

1. P. C. Gehlen and G. T. Hahn, Final Report on "Implications of Alloy Structure With Respect to Mechanical Properties" from Battelle-Columbus Laboratories to Office of Naval Research, Contract N00014-70-0390 (April 12, 1976).
2. P. C. Gehlen, A. R. Rosenfield, and G. T. Hahn, "Structure of the <100> Edge Dislocation in Iron", *J. Appl. Phys.* 39 (1968) 5246.
3. M. R. Louthan, Jr., G. R. Caskey, Jr., J. A. Donovan, and D. E. Rawl, Jr., "Hydrogen Embrittlement of Metals", *Mater. Sci. Eng.* 10 (1972) 357.
4. L. R. Kahn, unpublished work on "Quantum Chemical Calculations of Interatomic Potentials for Computer Simulations of Solids", Grant NSG-2027 to Battelle-Columbus Laboratories from NASA-Ames Research Center.
5. A. J. Markworth, M. F. Kanninen, and P. C. Gehlen, "An Atomic Model of an Environmentally-Affected Crack in BCC Iron", to be published in *Proc. Intern. Conf. on Stress Corrosion Cracking and Hydrogen Embrittlement of Iron Base Alloys* (Unieux-Firminy, France, June 10-16, 1973).
6. J. H. Walker, T.E.H. Walker, and H. P. Kelly, "Ground and Low-Lying Excited Electronic States of FeII", *J. Chem. Phys.* 57 (1972) 2094.
7. P. C. Gehlen, A. J. Markworth, and L. R. Kahn, "Atomistic Studies of Hydrogen-Enhanced Crack Propagation in BCC Iron", in Computer Simulation for Materials Applications (*Nucl. Metall.*, Vol. 20, Part 2, 1976), Edited by R. J. Arsenault, J. R. Beeler, Jr., and J. A. Simmons, p. 684.
8. D. R. Olander, "Description of the Hydrogen-Metal Interaction by a Morse Potential Function", *J. Phys. Chem. Solids* 32 (1971) 2499.
9. R. A. Johnson, "Point-Defect Calculations for an fcc Lattice", *Phys. Rev.* 145 (1966) 423.
10. S. N. Zhurkov, "Kinetic Concept of the Strength of Solids", *Intern. J. Fracture Mech.* 1 (1965) 311.
11. J. E. Sinclair, "Atomistic Computer Simulation of Brittle-Fracture Extension and Closure", *J. Phys. C: Solid State Phys.* 5 (1972) L271.
12. J. E. Sinclair and B. R. Lawn, "An Atomistic Study of Cracks in Diamond-Structure Crystals", *Proc. Royal Soc. London A* 329 (1972) 83.
13. C. Hsieh and R. Thomson, "Lattice Theory of Fracture and Crack Creep", *J. Appl. Phys.* 44 (1973) 2051.

14. E. Smith, "Effect of the Discreteness of the Atomic Structure on Cleavage Crack Extension in Brittle Crystalline Materials", *J. Appl. Phys.* 45 (1974) 2039.
15. J. E. Sinclair, "The Influence of the Interatomic Force Law and of Kinks on the Propagation of Brittle Cracks", *Phil. Mag.* 31 (1975) 647.
16. B. R. Lawn, "An Atomistic Model of Kinetic Crack Growth in Brittle Solids", *J. Mater. Sci.* 10 (1975) 469.
17. H. Hübner and W. Jillek, "Sub-Critical Crack Extension and Crack Resistance in Polycrystalline Alumina", *J. Mater. Sci.* 12 (1977) 117.
18. S. V. Tsivinsky, "Thermal Fluctuation Theory of Durability of Solids", *Mater. Sci. Eng.* 26 (1976) 13.
19. G. C. Sih and H. Liebowitz, "Mathematical Theories of Brittle Fracture", in Fracture—An Advanced Treatise, Edited by H. Liebowitz, Vol. II (Academic Press, New York, 1968), p. 67.
20. J. E. Sinclair and R. Fletcher, "A New Method of Saddle-Point Location for the Calculation of Defect Migration Energies", *J. Phys. C: Solid State Phys.* 7 (1974) 864.
21. R. Fletcher and C. M. Reeves, "Function Minimization by Conjugate Gradients", *Computer J.* 7 (1964) 149.
22. P. C. Gehlen, R. G. Hoagland, J. P. Hirth, and J. E. Sinclair, "Flexible Boundary Conditions and Nonlinear Geometric Effects in Atomic Dislocation Modelling", submitted to *J. Appl. Phys.*

APPENDIX A

Reprinted from Computer Simulation for Materials Applications (Nucl. Metall., Vol. 20, Part 2, 1976), Edited by R. J. Arsenault, J. R. Beeler, Jr., and J. A. Simmons, p. 684.

## ATOMISTIC STUDIES OF HYDROGEN-ENHANCED CRACK PROPAGATION IN BCC IRON

Pierre C. Gehlen, Alan J. Markworth, and Luis R. Kahn  
Metal Science Section, Battelle's Columbus Laboratories, Columbus, Ohio 43201

### Abstract

Results are presented of atomistic calculations of the effects, on crack propagation in body-centered-cubic iron, of hydrogen atoms located at the crack tip. The Fe-Fe interaction was described in terms of the Johnson interatomic potential, whereas an interatomic potential developed by Olander was used to describe the Fe-H interaction. The H-H interaction was not considered.

Calculations were carried out using both rigid and flexible boundaries and similar results were obtained for the two cases. Although the presence of hydrogen at the crack tip did indeed result in an enhancement of crack propagation relative to the situation in which hydrogen was not present, the degree of enhancement was found to be relatively insensitive to the level of externally applied stress. This contrasted sharply with the results of earlier calculations, based on a different Fe-H potential, in which effects of the presence of hydrogen were found to vary considerably with the applied-stress level. The differences in these sets of results are indicative of the existing need for accurate interatomic potentials.

### Introduction

The technological importance of environmentally assisted crack propagation is indeed immense, yet the state of our understanding, at a quantitative level, of the phenomena contributing to this effect, is relatively primitive. In particular, the development of models to describe the detailed nature of the discrete, atomic structure at the tip of a crack, which is under the influence of externally applied stress and is perhaps affected by the presence of foreign atoms, has become a practical possibility only with the advent of large-scale computers. Preliminary atomistic calculations have been reported elsewhere (1) concerning effects of hydrogen on crack propagation in  $\alpha$ -iron. It was thus found that the effect of a hydrogen atom, situated at the crack tip, was essentially to shorten the distances separating the four iron atoms which surrounded it; consequently, other Fe-Fe bonds were elongated and finally broke, one at a time, at a load that was about 10 percent lower than the normal load for failure of  $\alpha$ -iron. A major

shortcoming of this earlier work resulted from the fact that the Fe-H interatomic potential that was used was based on calculations performed for the FeH molecule. The research described herein consisted of additional atomistic calculations of the effects of hydrogen on crack propagation in  $\alpha$ -iron; these calculations were based, however, upon a different Fe-H potential than the one used in the earlier work. The present potential characterizes the pairwise interaction between a hydrogen atom and an atom of iron which is a constituent of the alpha phase of the metal.

#### The Fe-H Interaction Potential

Properties of Fe-H systems have been the subject of an extensive amount of research and have thus been widely discussed in the scientific literature. Of particular importance for atomistic simulation studies is the interaction potential between a hydrogen atom, situated within the iron lattice, and any given iron atom.

Interaction potentials for the FeH molecule have been ascertained. Thus, for example, gas-phase spectroscopic data have been used (2) for certain of the first-row transition-metal hydrides other than FeH to determine, by interpolation, appropriate Morse-function parameters for FeH. Also, Walker *et al.* (3) used many-body perturbation theory to execute approximate Hartree-Fock calculations describing a number of electronic states of the FeH molecule; and previously described simulations (1) of the effects of hydrogen on crack propagation in  $\alpha$ -iron were based on the data of Walker *et al.* (3) for the ground-state configuration.

The solubility of hydrogen in bulk face-centered-cubic metals (including the gamma phase of iron) has been described by Vykodets *et al.* (4) based on a Morse-function pairwise potential for the hydrogen-metal interaction. A Morse pairwise potential has also been used by Olander (5) to describe hydrogen-metal interactions. In Olander's work, experimentally determined values for heat of solution, heat of adsorption, and activation energy for bulk diffusion, all for hydrogen in the pertinent metals, were used to determine values for the Morse-function parameters for the various hydrogen-metal interactions. It was an Olander Fe-H potential which was used in the present study, i.e.,

$$V(r) = D \left\{ \exp \left[ -\frac{2m}{r_e} (r - r_e) \right] - 2 \exp \left[ -\frac{m}{r_e} (r - r_e) \right] \right\}$$

where  $V(r)$  is the Fe-H interaction energy at separation distance  $r$ , with  $r_e/a = 1.12$  ( $a$  being the lattice parameter, about 2.86 Å for body-centered-cubic iron),  $m = 2.96$ , and  $D = 4.6$  Kcal/mole (0.20 ev). This potential was determined for a {100} surface although values for these parameters were found to vary only to a minor degree with choice for the adsorption plane. For our calculations, the potential was set equal to zero for Fe-H separation distances greater than about 20 Å.

It should be noted that fundamental studies of the interaction between hydrogen and metals are continuing and these will yield added significant insights into this very important problem. Thus, for example, Ying *et al.* (6) have developed a density-functional theory of chemisorption using a self-consistent linear-response formalism and have applied their analysis to the case of hydrogen chemisorbed on a tungsten surface. The interaction energy between the hydrogen ion and the metal surface was determined as a function of distance of the ion from the surface. Likewise, interatomic forces are being calculated by Kahn (2) using a novel theoretical approach based on recent advances in the field of quantum chemistry. Kahn's initial calculations have been directed toward determining interatomic forces associated with a cluster of 10 iron atoms. Plans for refining this quantum-mechanical approach (2) include detailed comparisons between selected calculable and experimentally measurable bulk properties such as bulk modulus, elastic constants, structure factors, and Compton profiles. Calculations of interatomic forces associated with foreign atoms (such as hydrogen) contained within the metal will also be included.

#### Computational Procedure

The computer algorithm utilized in this study was formulated in order to obtain solutions of the Newtonian equations for a set of  $N$  atoms (considered to be point masses) in the immediate vicinity of a defect. It is usually convenient to start the computation by displacing the atoms from their perfect lattice positions according to the equations of linear elasticity for the given defect (in this particular case the linear anisotropic formalism of Sih and Liebowitz (7)). Once the atoms are so positioned, the net force on each atom can be evaluated and inserted into the equations of motion. These equations are then solved numerically until a stable minimum in the potential energy is obtained, or equivalently, until the force acting on every one of the  $N$  atoms is arbitrarily small. A complete description of the algorithm is given in Reference 8.

The present work applies to a crack length of  $2c$  that is embedded in a large continuum to which a load  $\sigma$  is applied in the <100> crystallographic direction. The crack plane is a {100} plane and the crack line is in the <001> direction.

Since we restrict ourselves to the case of plane strain (i.e., all displacements in the  $z$  direction are zero) the crystallographic periodicity is maintained along the crack line. Thus, by studying atomic displacements in only one crystallographic repeat distance containing two consecutive {001} planes, the crystal can be made infinite along the crack line by using periodic boundary conditions which permit simultaneous motion of equivalent atoms.

The discrete region contains about 700 atoms. If macroscopic properties of a body are to be simulated, this region must be surrounded by a much larger continuum with which it interacts. The interface between the two regions is referred to as a flexible

boundary. In essence, the flexible-boundary scheme, FLEX II, allows the continuum to accommodate nonlinear effects arising in the immediate vicinity of the crack tip. This scheme is described below.

After all atoms have been displaced in accord with principles of linear elasticity, the body containing the crack line is divided into a discrete atomic region (I), a boundary region (II), and a surrounding elastic continuum (III). The boundaries between the three regions are cylindrical, the axis of each cylinder being the crack line.

The essential properties of the three regions are as follows: Region I is comprised of a discrete array of atoms that contains the defect's center. Here the net interatomic forces are relaxed by integrating the equations of motion of the atoms. The atoms in Region II provide the link between Region I and the continuum. Here net forces are also calculated atomistically but the relaxation of these forces is accomplished by appropriate linear elastic displacement fields. The continuum, Region III, contains only the necessary complement of atoms for calculating the forces in Region II.

The computation scheme proceeds as follows: atoms only in Region I are relaxed for a period of time approximately equal to the time required for a sound wave to travel from the crack line to the interface between I and II and back. During this period the boundaries remain fixed. At the end of this interval the net forces on each atom in Region II are calculated using the interatomic potential. Because periodic boundaries are used along the crack line, these atomic forces can be converted directly to line forces with their line directions parallel to the crack line. With these forces known, atoms in all three regions are displaced using the linear elastic theory described in Equations 5 and 6 of Reference 9.\* These two steps are repeated alternately until finally the forces acting on the atoms in both Regions I and II have become vanishingly small at which point final equilibrium throughout the entire solid extending to infinity has been reached.

The load is applied to the discrete region by choosing the appropriate atomic displacements for the starting linear elastic configuration. The atomic displacements are proportional to the stress intensity factor for plane strain,  $K_I$ , which is given by

$$K_I = \sigma/\pi c \quad ,$$

where  $c$  is half the crack length and  $\sigma$  is the stress applied to the body. If a body containing a crack is perfectly brittle, a statement of the "Griffith principle" is that

\*The linear elastic scheme breaks down in the immediate vicinity of the point where the force is applied. The displacement of this point must be determined numerically.

crack extension occurs when the summation of the change in the elastic strain energy in the body plus the work done on the body during crack extension is equal to the energy required to form the new surfaces at the crack tip. The corresponding critical Griffith value of  $K_I$ , namely  $K_{IG}$ , was found to be  $0.77 \text{ MNm}^{-3/2}$ .

### Results

The computations described herein constitute an extension of earlier work (1) which was based on the potential developed by Walker *et al.* (3) for the FeH molecule. This potential (3) was characterized by a minimum energy value of  $19600 \text{ cm}^{-1}$  (i.e., 2.43 ev or 56.0 Kcal/mole) which was found, via their calculations (3), to exist at an interatomic separation of  $1.49 \text{ \AA}$ . These results can be compared to the Olander potential (5) used in the present work for which these same two parameters were quite different, i.e., 0.20 ev and  $3.21 \text{ \AA}$ , respectively. Shown in Figure 1 are results of a sample calculation from the earlier work showing the lattice distortion caused by the hydrogen atom, i.e., attracting the 4 iron atoms around it and thus elongating the Fe-Fe bonds beyond.

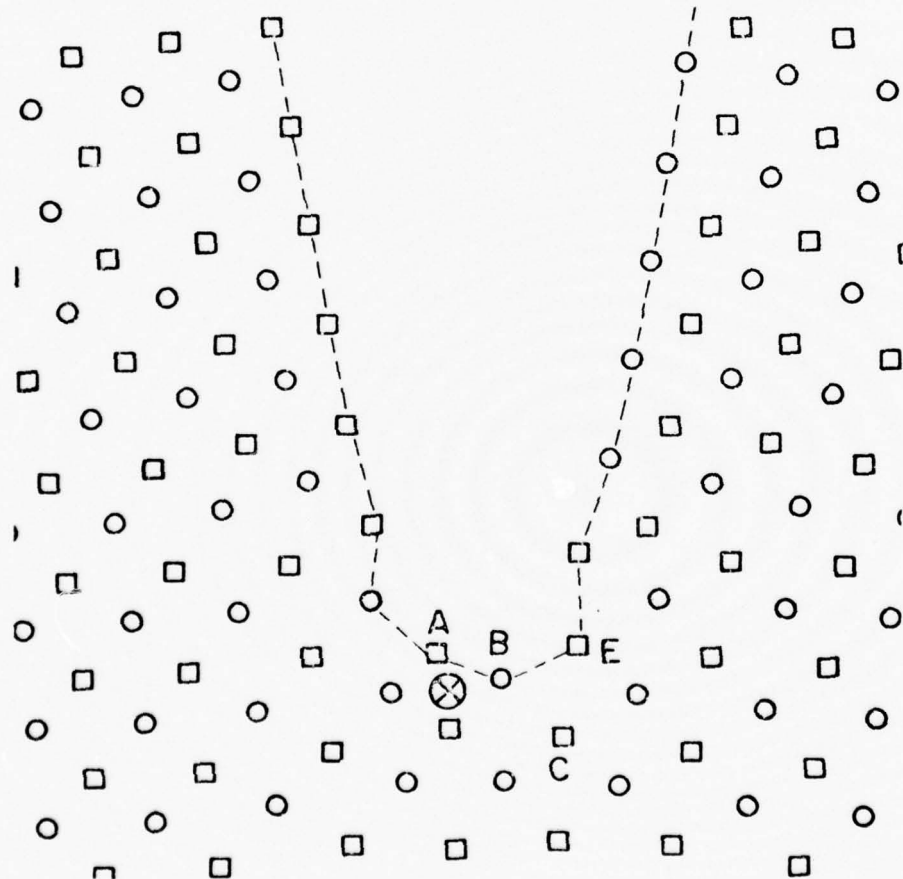


FIG 1

Distortion Around Crack Tip Based on Potential of  
Walker *et al.* (3) for the Fe-H Interaction (from Reference 1)

As can be seen in this figure, the hydrogen atom is closely surrounded by its four nearest-neighbor iron atoms. The left-ward motion of atom B causes bond BE to be stretched and eventually to break. In a similar computation without the hydrogen present, bond BE is not broken until the stress on the crystal is raised to  $K_I = 3.33 K_{IG}$  at which point unstable crack propagation occurs, the cleavage plane being the experimentally observed {100} plane. The embrittling effect of hydrogen is not evident for load levels less than  $K_I = 1.85 K_{IG}$ . These observations substantially agree with experimental observation. Subsequent computations, however, showed that the Walker *et al.* potential did not reproduce many of the known bulk properties of hydrogen in iron. For instance, it predicts a heat of solution about an order of magnitude larger than experimentally observed and a slightly negative molar volume, which is experimentally known to be positive. In an effort to correct these discrepancies, Olander's potential was substituted for Walker's. The former had been matched (5) to the heat of solution, resulting in its shallower well depth. Although the molar volume was not recalculated for the new potential, the position of the minimum in Olander's potential curve strongly indicates that the molar volume will be positive. Furthermore, the computer algorithm was improved by incorporating a new flexible boundary scheme which takes into account the fact that the crystal is a non-homogeneous (i.e., a cracked) body. In the previous calculation, the linear elastic formalism used to find the displacements associated with the forces in Region II (see above) was for a homogeneous body and the scheme used to make the crack stress-free was only approximate. In the present scheme, this boundary condition is satisfied rigorously. Finally, the range over which the hydrogen and iron atoms interact was extended from 4 Å in the old model to about 20 Å in the present model.

Results obtained from using the new computer algorithm and the Olander potential (5) are presented in Figures 2 through 4, all of which represent relaxed atomic configurations. In particular, illustrated in Figure 2 is a crack configuration, with no hydrogen present, and with  $K_I = 2.22 K_{IG}$ , whereas in Figure 3 and 4 are cracks containing hydrogen with  $K_I = 2.22 K_{IG}$  and  $1.48 K_{IG}$ , respectively. Comparison of Figures 2 and 3 shows that the hydrogen causes severe distortion of the lattice in its vicinity, the position of the crack tip (as defined by the line segments joining iron atoms at the surface along the crack) being markedly widened resulting from the presence of the hydrogen. Interestingly, it is the repulsive portion of the potential which dominates the effect in this work whereas it was the attractive portion which dominated the effects found in the earlier work (1).

When the Olander potential was used, it was found that even though the hydrogen atom was placed originally well within the iron lattice, the iron lattice appeared to "reject" the hydrogen atom and position it outside its surface. In the original Walker computation, the opposite occurred, namely, the starting position of the hydrogen atom was just outside the iron lattice and during relaxation the atom was moved to its position

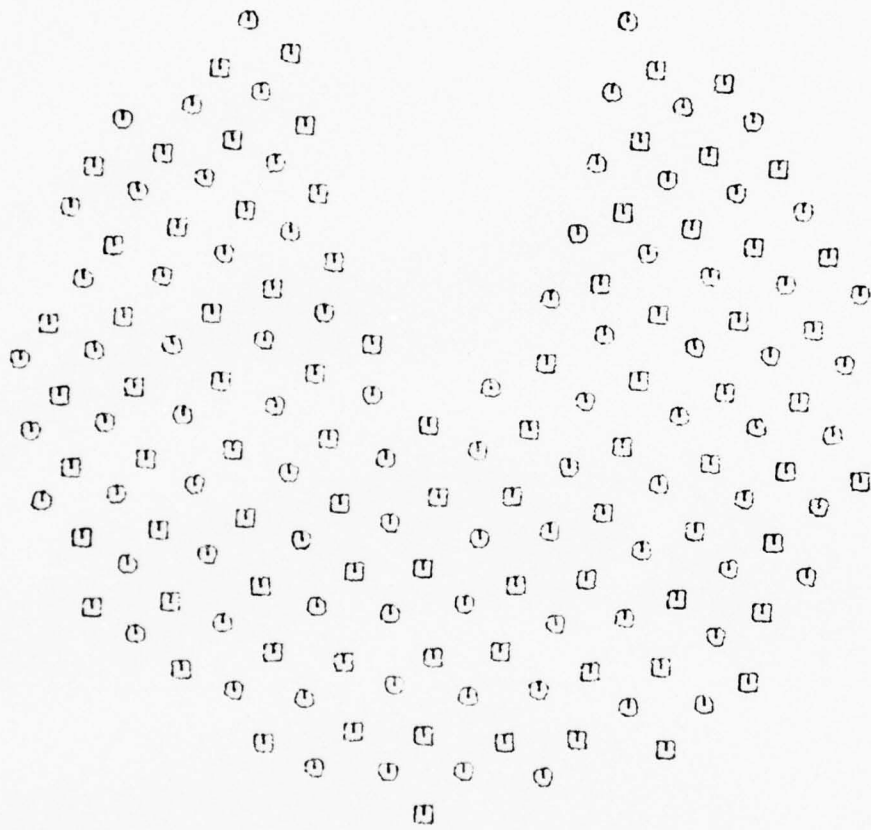


FIG 2  
Atomic Configuration Around a Crack Tip at  $K_I = 2.22 K_{IG}$

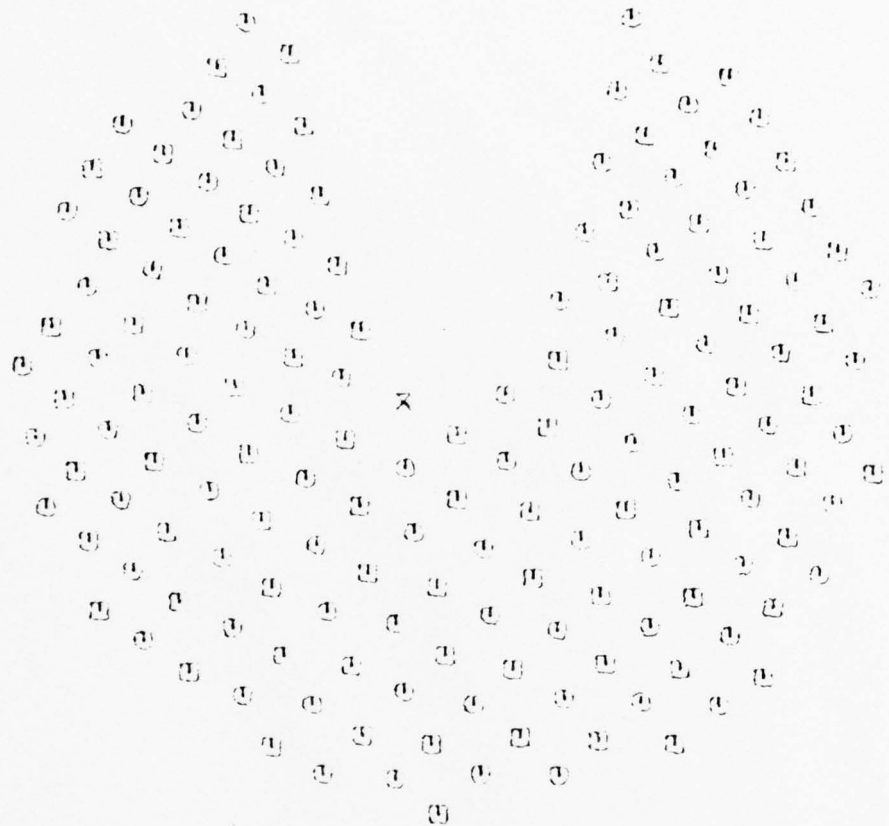


FIG 3  
Effect of Hydrogen (the H Atom Position Denoted by x)  
on the Crack Configuration for  $K_I = 2.22 K_{IG}$

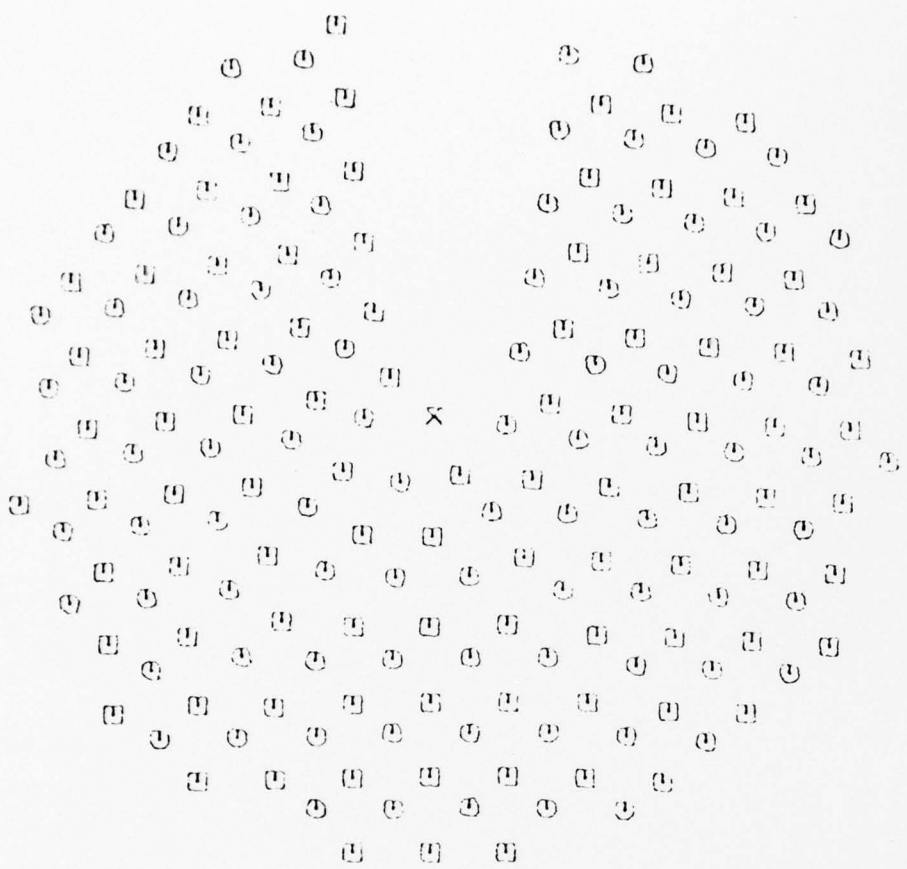


FIG 4  
Effect of Decreasing the  $K_1$  Value to  $1.48 K_{IG}$

shown in Figure 1. Originally it was thought that this rejection of the hydrogen was an artifact of the relaxation techniques, i.e., since the bottom of the well of the Fe-H interaction occurs at 3.21 Å (compared to an equilibrium distance of approximately 1.43 Å in an uncracked lattice), extremely large repulsive forces could act on the hydrogen atom during the first few relaxation steps, when the atom is at some distance from its equilibrium position within the iron lattice. In an effort to correct this situation, several attempts were made to dampen the atom's motion by increasing its mass by two orders of magnitude. This dampening had no effect on the end result, indicating that the configurations shown in Figures 3 and 4 are indeed the true equilibrium configurations corresponding to the Olander Fe-H interaction. Comparing Figures 3 and 4, we find that the effect of increasing the  $K_1$  value from  $1.48 K_{IG}$  to  $2.22 K_{IG}$  is to increase the crack-tip distortion brought about by the hydrogen to an even greater degree, as one would have expected. However, no Fe-Fe bonds were broken by increasing the  $K_1$  value to this higher level. Along these lines, we note that in the results of the previous work (1), elongated bonds did indeed break, one at a time, as the  $K_1$  value was increased.

### Conclusions

As we have already described, the effects of hydrogen on the nature of crack propagation in  $\alpha$ -iron were quite different in the earlier work (1), compared to those presented here. In the former case, Fe-Fe bonds broke, one at a time, as the  $K_I$  level was increased. In the latter situation, bond breakage occurred upon introduction of hydrogen into the lattice, and the effect of increasing the  $K_I$  level was not to break additional Fe-Fe bonds, but only to increase the lattice-distorting effect at the crack tip caused by the presence of the hydrogen. Unfortunately, because of the very small, atomistic scale at which these computations were carried out, we have no direct experimental data relative to hydrogen-enhanced crack propagation in  $\alpha$ -iron that can help us determine which of the two sets of computations was the more physically realistic. Thus, the need for reliable Fe-H interatomic potentials must indeed be placed at a high level of priority. It appears that theoretical work of the type being carried out of Kahn (2) and Ying *et al.* (6) represent promising means for reaching this goal.

Of course, the computations described here and in the earlier work (1) constitute only a beginning of atomistic-level studies of environmentally-enhanced crack propagation. Other effects must also be considered, such as those resulting from distributing the hydrogen all along the crack surface, not just near the most advanced position of the crack tip, and those resulting from the presence of other elements, such as sodium, that may also enhance crack propagation.

### Acknowledgement

Financial support of this work by the Office of Naval Research is gratefully acknowledged.

### References

1. A. J. Markworth, M. F. Kanninen, and P. C. Gehlen, "An Atomic Model of an Environmentally-Affected Crack in BCC Iron", to be published in Proc. of the Intern. Conf. on Stress Corrosion Cracking and Hydrogen Embrittlement of Iron Base Alloys, held at Unieux-Firminy, France (June 10 to 16, 1973).
2. L. R. Kahn, Metal Science Section, Battelle's Columbus Laboratories, Columbus, Ohio, work not as yet published.
3. J. H. Walker, T. E. H. Walker, and H. P. Kelly, J. Chem. Phys. 57, 2094 (1972).
4. V. B. Vykhodets, V. B. Demin, P. V. Gel'd, A. N. Men', A. Ya. Fishman, and G. I. Chufarov, Russian Metallurgy, No. 6, 55 (1971).
5. D. R. Olander, J. Phys. Chem. Solids 32, 2499 (1971).
6. S. C. Ying, J. R. Smith, and W. Kohn, Phys. Rev. B 11, 1483 (1975).

7. G. C. Sih and H. Liebowitz, Fracture, An Advanced Treatise, Vol. II, Mathematical Fundamentals, Edited by H. Liebowitz, p. 67, Academic Press, Inc., New York (1968).
8. P. C. Gehlen, A. R. Rosenfield, and G. T. Hahn, J. Appl. Phys. 39, 5246 (1968).
9. J. P. Hirth, R. G. Hoagland, and P. C. Gehlen, Intern. J. Solids and Structures 10, 977 (1974).

APPENDIX B

Submitted to Journal of Applied Physics

Flexible Boundary Conditions and Nonlinear Geometric Effects  
in Atomic Dislocation Modelling

by

P.C. Gehlen, R.G. Hoagland, J.P. Hirth and J.E. Sinclair

Abstract

A technique, Flex-II, is described for applying flexible boundaries to an atomic region in computer simulation of dislocations or other line defects. The method results in continuity of equilibrium, under the chosen interatomic potential, across the interface between the atomic region and the outer region described in terms of anisotropic elastic continuum solutions. The technique has high numerical efficiency. It is shown that when the crystal is initially dislocated according to the Volterra solution for displacements, the finite strains give rise to geometrical nonlinear effects, usually disregarded in linear elasticity, which contribute to a volume change of the crystal. Allowance for this effect, and for elastic nonlinearity in the crystal beyond the boundary region, allow the overall dilatation of a finite body due to the dislocation to be rigorously computed. For illustration of the geometric nonlinear effect, and for comparison with earlier modelling methods, example computations are given for the [100] edge dislocation in  $\alpha$ -iron.

## I. Introduction

In atomistic computer models of crystal defects such as dislocations or crack tips, incompatibilities at the boundary of the atomic region will arise unless a "flexible boundary" scheme is employed. Several such methods<sup>(1-3)</sup> have recently been developed, and have improved the efficiency of the calculations by permitting the use of smaller atomic arrays, have yielded descriptions of the dilatational and higher-order elastic fields arising from nonlinearity in the core region, and have made possible calculations of defect mobility by removing the constraints imposed by rigid boundaries. Various modified versions of the flexible boundary methods have been briefly described<sup>(4,5)</sup>. Furthermore, our current work has revealed some subtleties in the interpretation of the core contribution to the field of a dislocation, connected with the finite nature of the strains in the initial Volterra-solution configuration. These geometric nonlinear effects lead to revision of the earlier descriptions of dislocation core field strengths, although the final configurations previously determined are not affected.

In view of these changes in both method and interpretation, we here present the details for the evolved form "Flex-II", which we have found to be most efficient for computer defect calculations, and spell out the steps required to form an accurate representation of the elastic field strengths, including volume change, associated with a dislocation core. A brief comparative account is given of earlier flexible boundary methods. Some selected results are presented to permit comparison among the models.

## II. Computational Procedure

### A. Flex-II

The method consists of a number of steps, for most of which certain alternatives exist as to detailed procedure. In some cases, the choice is a matter of taste or convenience. Somewhat surprisingly however, in the step of setting up initial positions, what appear at first sight to be arbitrary alternatives lead to important differences in effect. For clarity, we first give the basic sequence of steps and then discuss each step, with any alternative options, in turn. Although the method is applicable to dislocations, crack tips, and other straight line defects, for brevity the description is given primarily for the dislocation case.

The first step is to generate an array of atom positions for a block of perfect lattice, one crystallographic repeat distance thick in the  $x_3$  direction (along which the dislocation is to lie), and of sufficient size in the  $x_1$  and  $x_2$  directions to accommodate the regions chosen later in the dislocated crystal. This straightforward step will not be dwelt upon except to remark that the choice of a high index direction for  $x_3$  can result in the formation of a series of jogs or kinks<sup>(6)</sup>, if study of these is desired.

The next step is to form an initial dislocated configuration by displacing all atoms according to a linear-elastic displacement field. This will be discussed in more detail below. The resulting array is then divided into three parts, as in Figure 1.

Region I contains those atoms (in reality, atom rows) which are to be relaxed independently because their interactions, according to the chosen interatomic potential, are substantially nonlinear. Atoms in regions II and III interact via the same potential, but they are always displaced collectively, according to elastic Green functions. Region II contains all atoms on which a force may be exerted by at least one region-I atom, while region III is that portion of the remainder of the crystal which is necessary to fully define the force on each region-II atom. The thickness of both regions II and III should thus equal the maximum range of the interatomic force law. Many empirical potentials for metals have been formulated<sup>(7-10)</sup> with a specific cut-off at less than the fourth nearest neighbour distance. An artificial cut-off must be used for longer-ranged, e.g. ionic, potentials<sup>(3-5)</sup>. The shape of region I may conveniently be chosen as either a circular cylinder centered on the dislocation, or as a roughly square block aligned with the distorted crystal planes.

The following final two steps are repeated alternately. The first is to relax the atoms of region I towards their equilibrium state according to the atomic force law. Since later steps will disturb the region by changing the boundary conditions, this relaxation stage is not, for efficiency's sake, greatly prolonged in search of precise equilibrium. If a modest limit (e.g. 50) is set for this step on the number of force calculations allowed, then in early iterations a useful economy is obtained, while in the final iteration a sufficiently precise equilibrium results, since the final relaxation is only a small adjustment.

The second of the iterated steps is to use the forces still remaining on region -II atoms to generate a corrective displacement field for all three regions (and, implicitly, the entire crystal), composed from a superposition of Green functions. In this two-dimensional context, a Green function for a lattice or continuum is a displacement field which will produce equilibrium in response to a line of force of unit strength in a chosen direction, applied at some origin. (Alternately, the same displacements remove a line of force existing through internal interactions). It is thus necessary in this step of the calculation to form a sum of Green function fields with origins at each of the region-II atoms, and source strengths given by the forces on those atoms, first converted to units of force per unit  $x_3$ -length. Because region I is nonlinear and inhomogeneous, this step, which uses the Green function for an infinite homogeneous body, cannot produce exact equilibrium. Iteration of the final two steps is thus necessary. However, to the extent that regions II and III behave linearly, no forces requiring correction by Green functions should ever develop in region III or beyond, for all the interacting neighbours of any atom in region III are displaced only according to equilibrium linear-elastic fields.

The two final steps should be iterated until no atom in regions I or II has a resultant force greater than some chosen tolerance. Convergence in 3 to 6 iterations is usual in our experience. During the iterations, it is useful to accumulate certain information on the source strengths of the Green function

displacements applied, for use in analysis of the dislocation core field. This will be discussed in section II B, after the following enlargements on the alternative options available at each step.

#### Initial positions from linear elasticity

Regarding the choice between isotropic- and anisotropic-elasticity solutions for the field of a dislocation, we believe that the latter results should be used in all cases. Although trials have shown little effect on core structure from using the inappropriate, but analytically simpler, isotropic expressions, the anisotropic results are now well documented, and new, numerically efficient methods of computing them have become available. Arbitrary orientations and anisotropy can most expediently be dealt with using the so-called integral formalism<sup>(11)</sup>. Alternatively, for high-symmetry cases, the "sextic" formalism<sup>(12,13)</sup> using complex functions, leads to simple expressions which may be easier to implement if great generality is not required. All of these solutions, whether isotropic or anisotropic, we shall loosely term "Volterra fields", meaning that only the dominant, logarithmic singularity is included.

A second question which has received discussion in previous dislocation modelling work, is the possible unexpected asymmetry which can occur when the Volterra solution for an edge dislocation is applied in the most obvious way. This can arise because the linear elasticity theory, being based on an infinitesimal

strain measure, does not distinguish the geometry of the initial and distorted states. Thus, the loss of symmetry which occurs for edge dislocations when the Volterra solution is taken as a function of initial, or Lagrangian coordinates, is not "noticed" by the infinitesimal theory. It happens that this asymmetry can be avoided if the branch cut, or surface of discontinuity in the Volterra field, is moved from the  $x_1$  axis to the positive  $x_2$  axis, corresponding to dislocation formation by insertion of a half-plane of atoms, rather than by slip. This was the approach used by Gehlen et al<sup>(2)</sup>. An alternative scheme<sup>(1)</sup> which results in the expected symmetry, is to use final-state, or Eulerian coordinates. To do this, it is simply necessary to iterate the calculation of the displacement of each atom until its displacement from the corresponding perfect lattice position is self-consistently given by the Volterra solution evaluated at the displaced position.

The choice from among the above, or other similar operational schemes for setting up initial positions, would appear at first sight to be arbitrary, since all are equally valid within the terms of the infinitesimal-strain, linear elasticity theory. However, when calculating the volume change associated with the core field which is found in the course of flexible boundary relaxation, it turns out that the small differences between the various above interpretations of the Volterra solution cannot be neglected, since they include a significant relative difference in dilatation, both local and overall. This is of second order in the strain magnitude; that is, of geometrical non-linear origin.

The well known result, that the Volterra solution causes no volume change, is true only to lowest order in the strain magnitude. The results of choosing different representations of the Volterra solution will be demonstrated in section IIIB. Whatever the choice, Flex-II produces an accurate equilibrium configuration. However, because of the greater ease in calculating the overall volume change (section IIB), we prefer to use the Eulerian coordinate approach to calculating initial positions.

#### Atomic Relaxation

We have used two different methods. One, the so-called dynamic method<sup>(14)</sup>, is well known and is based on an integration of the equations of motion, with periodic or continuous artificial quenching of the kinetic energy. The other, known as conjugate gradients<sup>(15,16)</sup>, is less mechanical in philosophy, and consists of a series of searches of configuration space, systematically reducing components of the energy gradient vector to zero. One or other of these methods may be more efficient for a given initial configuration and potential, but the difference in performance is never very great.

#### The Green Function

Because of the gross distortions in the core, the body is elastically inhomogeneous, and the true Green function depends on both source and field position. Neglect of this fact allows us more simply to use a function only of the relative source-field

position. But because of the dislocation, the relative positioning of two atoms cannot be uniquely defined in terms of lattice indices. It is therefore necessary, and in any case much simpler, to use a continuum Green function for moderate and large separations. The anisotropic elastic displacement field of a line force is given in the integral formalism by Asaro et al.<sup>(11)</sup> or in the sextic formalism by Stroh<sup>(13)</sup>. For high symmetry cases<sup>(17)</sup> or the isotropic approximation<sup>(2)</sup> simpler explicit expressions are available. All of these solutions diverge logarithmically at the line of force, so that they certainly cannot give the displacement of the row of atoms on which forces act, nor, probably, that of other closely neighbouring rows. However, the neighbourhood of any region-II atom is essentially perfect lattice, so that a lattice Green function may be used for near neighbours. This can easily be calculated by performing a relaxation of a small block of perfect crystal, with the central row of atoms bearing an externally applied force, and the boundary atoms being located according to the continuum Green function. The resulting displacements per unit applied force are stored in an array for use in Flex-II. The size of the atomic region which has to be relaxed in this subsidiary experiment in order to give good equilibrium will indicate the range at which the continuum Green function must be replaced by the lattice Green function. In model  $\alpha$ -iron, a range of about  $3b/2$  was found sufficient. In early work on Flex-II<sup>(3)</sup>, the need for a lattice Green function was neglected, zero value being associated with the row at the origin. Slow convergence was still achieved in the Flex-II procedure, but this

could not be guaranteed in general of course.

An alternative to pre-calculating the near-neighbour lattice Green function values is as follows. Only regions I and III are displaced in response to forces in region II, using the continuum Green function. The required displacements for region II are then obtained by relaxing the atoms in that region holding regions I and III fixed. This procedure was devised to deal with applications to cracks, where the Green function, including near-neighbour lattice values, is a function of source position relative to the crack faces.

#### B. Analysis of dislocation core field and volume change

At the completion of the Flex-II procedure, the displacement field of the entire crystal excluding region I is given by the Volterra field plus an additional field, related to the core conditions, comprising a sum of Green function terms. This core field can be completely described in terms of the total distribution of line forces which generate it. The properties of this distribution which relate to the elastic far field are the moments of the distribution about the origin. Of greatest significance are the dipole moments

$$M_{ij} = \sum_n F_i(n) x_j(n), \quad i, j = 1 \text{ or } 2 \quad (1)$$

where  $F(n)$  is the force per unit  $x_3$ -length at  $x(n)$ , the  $n$ -th atom-row position. If  $(x_2 x_3)$  is a mirror plane, only  $M_{11}$  and  $M_{22}$  will be non-zero. The dipole moments can be related to the dilatation of the body which the core-field terms contribute; higher order

moments give further information such as the positioning of the apparent core-field origin relative to the dislocation line (see sect. II D).

Unfortunately, as explained in the previous section, the definition of the Volterra field is somewhat arbitrary, so that the above characterization of the additional core-related field in terms of linear elastic solutions is not unique, but may only be given with respect to a particular representation of the Volterra field. Nevertheless, it is possible to determine uniquely such overall features as the formation volume of the dislocation, as we now describe. To do so, we must take into account not only the arbitrary choices made in constructing the Volterra field, such as origin and branch cut positions, but also both geometric and elastic non-linearities. However, it is not necessary to derive, nor to use in the relaxation, a complete non-linear-elastic solution for the field of a dislocation.

We may list the far-field terms contributing to the overall dilatation as:

- 1) the initial Volterra displacement field;
- 2) the Green-function terms applied to regions II and III during relaxation;
- 3) additional displacements which would be needed to achieve exact equilibrium throughout the material beyond region II; these are necessary because the nonlinear terms in the stress-strain law lead to both a body force distribution throughout

this outermost region, and to outer surface tractions, when the strains are given by linear elastic fields;

4) any misfit at the branch cut (slip plane) in the initial Volterra field.

Contribution (4) arises only when Lagrangian coordinates are used. A slight overlap of material results from failure of the Lagrangian Volterra solution to satisfy exactly the required displacement jump conditions on the slip plane. This oddity is scarcely noticed in the atomic modelling, but must be allowed for in order to obtain the same final result independent of the initial configuration. To avoid this complication, we restrict the following analysis to Eulerian coordinates, and give expressions for the three contributions to the overall volume change.

Firstly, in order to compare the volume of a body with the Eulerian Volterra displacements to that of the same quantity of material without dislocation, care must be taken to define the position of the slip surface, and furthermore, the following exact expression for the area change of a contour must be employed:

$$\delta A = \oint_{\ell} [ \tilde{u} \times d\tilde{\ell} ] - \frac{1}{2} \oint_{\ell} [\tilde{u} \times \frac{du}{d\tilde{\ell}}] d\tilde{\ell} \quad (2)$$

in which the first term is the customary infinitesimal strain result, and the second term enters because the material points connected by  $d\tilde{\ell}$  in the final state have a different separation in the initial state. In eq. (2),  $\ell$  is a closed contour in the

final state, and  $\tilde{u}$  is a displacement field expressed in terms of final coordinates. When applied to the Volterra field for an edge dislocation in a circular cylindrical body of radius  $R$ , equation (2) yields for the volume change per unit length

$$\delta A_{EV} = b^2 [\alpha_1 \ln(R/r_0) + \alpha_2] \quad (3)$$

Here  $b$  is the Burgers vector, taken to be in the  $x_1$  direction, and  $\alpha_1$  and  $\alpha_2$  depend on the elastic constants. For isotropic elasticity,

$$\alpha_1 = -\frac{1-2\nu}{4\pi(1-\nu)} ; \quad \alpha_2 = -\frac{5-4\nu}{8\pi(1-\nu)} , \quad (4)$$

where  $\nu$  is Poisson's ratio. For anisotropy,  $\alpha_1$  is simply the coefficient of  $b \ln r$  appearing in the  $x_2$ -displacement component; no expression for  $\alpha_2$  can be given, since it depends upon the form of the relaxation terms arising at a free cylindrical surface, presently unknown for anisotropy. The choice of slip surface position enters through  $r_0$ , in eq. (3), defined to be the distance from the origin at which the slip surface in the final state crosses the  $x_1$  coordinate axis. This may be altered, for instance, by shifting the atomic structure relative to the coordinate system in such a way that climb appears to take place without in fact altering the amount of material at the core.

Secondly, the volume change during relaxation by Flex-II, which we shall express as

$$\delta A_{CF} = b^2 \alpha_3 , \quad (5)$$

is given in terms of the dipole moments (eq. 1) by\*

$$\delta A_{CF} = S_{ijkl} M_{jk} \quad (6)$$

where

$$S_{ijkl} \equiv s_{ijkl} - s_{ij33} s_{33kl} / s_{3333}, \quad (7)$$

and  $s_{ijkl}$  are the anisotropic compliance constants appropriate to the chosen dislocation orientation. It is important to realise that this formula applies to a finite body. The "infinite body" dilatation, i.e. that of a large material surface far from both the defect and the free surface, is related to the  $M_{ij}$  by different compliances.

Finally, the volume change associated with hypothetical relaxation of the nonlinear-elastic effects beyond regions I and II can be found to sufficient accuracy by calculating the linear elastic relaxation of the remaining forces associated with nonlinear effects. In terms of the third order constants  $d_{ijklmn}$  defined by Willis<sup>(19)</sup>, the body force per unit volume, existing under Eulerian displacements  $u_i$  satisfying the linear-elastic equilibrium equation, is

$$f_i = d_{ijklmn} \frac{\partial}{\partial x_j} \left[ \frac{\partial u_l}{\partial x_k} \frac{\partial u_n}{\partial x_m} \right] \quad (8)$$

In terms of moments of this distribution defined by

---

\* This is the result for plane strain and anisotropy corresponding to the three dimensional, isotropic result given on page 89 of Eshelby (ref. 18).

$$M_{ij} = \int f_i x_j dA, \quad (9)$$

the finite-body volume change associated with linear-elastic relaxation of these forces is given by the same formula as eq. (6). In addition, the non-linear elastic law will lead to surface tractions whose relaxation would produce a further dilatation. Because we do not have, even for the simple case of a circular cylindrical body, exact expressions for the strains at and near the free outer surface (if the elasticity is anisotropic), the last mentioned contribution to the dilatation, and also part of the contribution from the body force (8), cannot be determined. However, the principal contribution from the nonlinear effects can be found by using the infinite body expression for the strains  $\partial u_\ell / \partial x_k$  in (8), which takes the form

$$\frac{\partial u_\ell}{\partial x_k} = \frac{1}{r} h_{k\ell}(\theta), \quad (10)$$

where  $r, \theta$  are polar coordinates. Substitution in (8) leads to

$$f_i(r, \theta) = r^{-3} g_i(\theta), \quad (11)$$

and finally, through (9), to the following form for the total non-linear elastic contribution to the dilatation:

$$\delta A_{NL} = b^2 (\alpha_4 \ln(R/r_1) + \alpha_5), \quad (12)$$

where  $r_1$  is the inner radius at which the integral (9) commences. Section III-C shows how the effective value of  $r_1$  can be

determined in practice, but clearly, it corresponds closely to the inner radius of region III. The value of  $\alpha_4$  is well determined through the second and third order elastic constants entering in (8) and (10). The unknown surface-relaxation effects are embraced by the term  $\alpha_5$ . Consideration of the order in  $r$  of the surface terms, and examination of the isotropic case, show that  $\alpha_5$  is independent of  $R$ . Hence this term could alternatively be embraced in the  $\alpha_4$  term by taking an "effective" value for  $R$ . In the practical case of a body containing many dislocations,  $R$  can in any case only be estimated in terms of the average spacing of dislocations.

By adding (3), (5) and (12), we obtain for the total volume of formation per unit length of dislocation

$$\delta A_{\text{tot.}} = b^2 [\alpha_{\text{core}} + \alpha_{\text{NL}} \ln(R/b) + \alpha_{\text{outer}}], \quad (13)$$

where

$$\alpha_{\text{core}} = \alpha_3 - \alpha_1 \ln(r_0/b) - \alpha_4 \ln(r_1/b), \quad (14)$$

$$\alpha_{\text{NL}} = \alpha_1 + \alpha_4, \quad (15)$$

$$\alpha_{\text{outer}} = \alpha_2 + \alpha_5 \quad (16)$$

In (13) we have chosen  $b$  as the most natural scaling length for expressing the logarithmic term. The core related term  $\alpha_{\text{core}}$  is then given by the model-relaxation term  $\alpha_3$  (given by eqs. 1 and 6) "corrected" for the effects of arbitrary model parameters  $r_0$  (which reflects the relative positioning of atomic structure and coordinate system) and  $r_1$  (the radius of the relaxed region).

The  $\alpha_{NL}$  term reflects the elastic properties, linear and non-linear, of the material, while the last term includes the effects of the outer boundary conditions. Again, this term could be incorporated in the second by suitable choice of an effective value for R.

### C. Other Flex Methods

The first flexible boundary method, which we shall call Flex-S, was developed by Sinclair<sup>(1)</sup>. In that method, atoms in region II and beyond are displaced from their Volterra positions, not by Green functions, but by a truncated series of higher order elastic terms with multipole singularities at the dislocation line. The incompatibility forces in region II are converted into generalized forces on the higher term coefficients, and these forces with the atomic forces in region I are simultaneously relaxed. This fully anisotropic method gives results in good agreement with Flex-II. However, Flex-II has proved more efficient in computing time, by a factor of five, in the comparisons of section III and also in trials by Puls and Woo<sup>(5)</sup>. The original Flex-S calculations used a matrix method of relaxation, which required few force calculations, but expensive matrix manipulations. Later calculations using the more practicable conjugate gradients relaxation method required very many force calculations. The latter relaxation method appears to respond poorly to the particular type of disequilibrium which is generated at intermediate steps by the Flex-S system. Flex-S has, however, been used by Sinclair<sup>(6)</sup>

in crack modelling work and performed much more efficiently than in the dislocation case. The reason for the difference is not known.

Another flexible boundary method, developed at about the same time as Flex-S, was Flex-I<sup>(2)</sup>. Compatibility between the regions was sought by calculating the tractions acting across a circular path lying within region I, representing these by a Fourier series, and then imposing additional elastic displacements on the outer region, corresponding to the traction distribution. This method was developed only in the isotropic approximation. However, Teodosiu et al<sup>(20)</sup> have recently provided the necessary anisotropic elastic solutions, which Petrasch and co-workers<sup>(21-22)</sup> have used in a model which is essentially Flex-I starting from non-linear anisotropic initial positions. However, we have found Flex-I to be much less efficient than either Flex-S or Flex-II.

#### D. Extension to Cracks

For planar cracks with straight tips, essentially the same Flex-II technique can be applied. The major difference is that the Green function appropriate for a cracked body must be used. This has been given for general anisotropy in the sextic formalism by Sinclair and Hirth<sup>(23)</sup> and in the isotropic approximation by Hirth et al.<sup>(24)</sup>. The modifications necessary because of the non-availability of a general near-neighbour lattice Green function, have already been given at the end of section II A.

### III. Results

For purposes of comparison, we treat the [100] edge dislocation in bcc iron as represented by the Johnson-I potential<sup>(7)</sup>. This dislocation was already used as the example case for Flex-S<sup>(1)</sup> and Flex-I<sup>(2)</sup>.

#### A. Flex-II Efficiency

As an indication of the numerical efficiency of the method, we give an example of a typical calculation on the above dislocation. Region I contained 152 atoms, region II a further 78 atoms. The desired accuracy for convergence was that all forces be smaller than  $10^{-3}$  eV $\text{\AA}^{-1}$ . The conjugate gradient relaxation method (CGR) was used, with a limit of 50 on the calls to the force calculating routine. The history of the calculation was as follows. CGR (limit of 50 reached) on region I, left forces in region II of  $0.05$  eV $\text{\AA}^{-1}$  typical; Green functions applied; CGR (39 force calls): region-II forces  $0.005$  typical,  $0.02$  maximum; Green function applied; CGR(16); Green functions; CGR(5); all forces in regions I and II now less than  $10^{-3}$  eV $\text{\AA}^{-1}$ ; total force calls = 110. For comparison a run of Flex-S on the same model required 426 force calls for the same accuracy. The original Flex-I calculations typically required over 1000 force calculations.

#### B. Core Configuration

The dislocation core configurations generated by different computational algorithms can be compared in terms of the distances

between atom pairs closest to the core that are most affected by the relaxation. Table I presents a few selected interatomic distances for the rigid boundary, Flex-S, Flex-I and Flex-II models. The atom pairs are those depicted in figure 2. The results of the various flexible boundary treatments are in good agreement with each other and with the large rigid boundary model. The small differences between the flexible models are attributable to the varying termination criteria for the relaxation procedures, and to the small residual errors at the boundary, which differ according to the linear elastic approach and region shape in use. As found in previous work,<sup>(1,2,25)</sup> the effect of using isotropic rather than anisotropic elasticity in the boundary conditions is not large; the core configuration is determined principally by the choice of potential.

Although not displayed in Table I, the dependence of core atom spacings on model size, using Flex-II, is very small (<0.05%) down to about 100 atoms in region I, just as was found with Flex-S<sup>(1)</sup> and Flex-I<sup>(2)</sup>. By contrast, with rigid boundary conditions, the core atom spacings vary by several percent for region I in the range 90 to 780 atoms<sup>(1,2)</sup>.

### C. Dilatation with Different Volterra Field Representations

One of the aims of the present work was to resolve a puzzling apparent inconsistency between the Flex-S and Flex-I models with respect to the dilatational effect of the core. From the published values of the higher-term coefficients in the relaxed Flex-S boundary, one can calculate the area expansion of a

circular path in the continuum region, centered on the dislocation. The result, for the change from the Volterra configuration to the final relaxed state, is  $\delta A = 0.45b^2$ . The same quantity was measured directly in the Flex-I model from the atomic displacements, with the result  $\delta A = 0.25b^2$ . In confirmation, the (unpublished) coefficients of the higher terms in the Flex-I boundary fields lead to the value  $\delta A = 0.27b^2$  in the continuum region.

In the light of the analysis in section IIB, we now recognise that this difference originates from the geometric nonlinear volume change associated with the change from perfect lattice to Volterra configuration. When Lagrangian coordinates are used (as in Flex-I), the exact initial configuration actually depends upon the angle at which the plane of discontinuity in the displacement field lies. With Eulerian coordinates, the angle of this branch cut is immaterial, but the configuration is still sensitive to arbitrary origin shifts which appear, from the far field, to be dislocation climb.

To fully investigate these effects, we have used Flex-II to perform relaxations from four different initial configurations, obtained from the anisotropic Volterra field by the means indicated in figure 3. The resulting relaxed configurations were almost identical, as revealed by the interatomic spacings not only near the core, but also in the boundary region. However, rather than comparing results in these terms, we display in Table II a quantity more directly related to the question of dilatation: the area of a local circuit enclosing the dislocation. The circuit chosen was roughly square, passing through a sequence

of atom rows just inside region 1. The reference perfect-lattice area is that for the same number of atoms as in the circuit, with edge and corner atoms counted fractionally. The results of Table II show firstly that the final configuration is, to good approximation, independent of the path taken to create and relax the dislocation. Secondly, it may be seen that the values quoted above for core dilatations in the earlier Flex-S and Flex-I calculations agree well with the relaxation area changes in the corresponding present results: compare case (d) with the original Flex-S result; case (a) with Flex-I. It is important to realise that the relative circuit area changes cannot be associated with the overall dilatation of the dislocated body, because

- (i) relaxation of the outer surface of the body leads to an overall dilatation different from that of a circuit far inside the surface;
- (ii) geometric and elastic nonlinearities outside the circuit contribute to the overall dilatation;
- (iii) the circuit is not, and indeed could not be, perfectly centered on the dislocation, so that even from an infinitesimal strain viewpoint, the Volterra field would contribute to the area change.

We now use the analysis of section II-B to calculate the total formation of the dislocation, using the Flex-II results and Eulerian coordinates. While doing so, we explore one further variation in the manner of creating initial positions. In

case (d) of Table II, atom positions in  $\text{\AA}$  were used in the logarithm functions of the Volterra displacement field. This choice of units is arbitrary, but changing the units adds a constant to the  $x_2$  displacement function, which in Eulerian coordinates amount to shifting the initial perfect lattice relative to the coordinate origin. This, through altering  $r_0$  defined following eq. (3), alters the volume of the dislocated initial configuration. Hence, to show that the final result is independent of this arbitrary choice, we made a further calculation in which a constant additional  $x_2$ -displacement of 0.1b was added to the Volterra field, equivalent to taking  $r_0 = 7.293\text{\AA}$  in equation (3). After completing the relaxation in each case, using Flex-II, the forces in region III were examined (extending the atomic structure as necessary) to check the transition to the distribution of forces predicted by nonlinear elasticity theory (eq. 8). When moments of these very small forces were calculated as in eq. (1), taking the sum out to a certain radius  $r$ , the variation of the sum with  $\ln r$  became linear, with the slope predicted from nonlinear elasticity, just as soon as the circle of radius  $r$  lay completely outside region II, which was square in shape. From the intercept of the graph against  $\ln r$ , the effective value of  $r_1$  in eq. (12) could be found. With circular regions in use,  $r_1$  could be taken as the inner radius of region III.

The results which enter into the total dilatation are shown in Table III. It can be seen that the effective shift of

origin by  $0.1b$  of the Volterra field with respect to the crystal lattice, leads to changes in the relaxation field (as represented by moments  $M_{11}$  and  $M_{22}$  and the dilatation parameter  $\alpha_3$ ) which almost exactly compensate for the difference of  $0.1b^2$  in initial dilatation, so that the total volume change, given by  $\alpha_{\text{core}}$  and  $\alpha_{\text{NL}}$ , is almost exactly the same. The final result, then, for the volume change per unit length of a cylinder of effective radius  $R$  (see Sect. IIB) upon creation of a dislocation on the axis, is  $\delta A = [0.37 + 0.070 \ln(R/b)]b^2$ . The result is, of course, dependent on the interatomic potential acting. For a typical effective value  $R = 10^4b$ , the result becomes  $\delta A = 1.01b^2$ .

In order to emphasize the importance of the results of this section, we offer the following physical description. The final configuration of a given group of atoms containing the dislocation is the same, independent of the method used to determine it. For example, in the explored adjustment of the initial configuration which involved an origin shift of  $0.1b$  in the climb direction away from the physically more obvious choice midway between two atom planes, initial interatomic forces were produced in region I such that upon relaxation the dislocation "climbed down" again. This in turn led to different flexible boundary relaxations, so that the relaxation volume change  $\delta A_{\text{CF}}$ , expressed by the parameter  $\alpha_3$  derived from region-II force dipole moments, was  $0.1b^2$  smaller. This difference in the relaxation volume was however almost exactly compensated by that in the non-linear geometric volume change involved in formation of the initial configuration. This

compensation is expressed by eq. (14), in which the term in  $r_0$  expresses the initial displacement, in the climb direction, of the apparent slip plane from the coordinate origin.

Because this careful analysis is necessary, it may be thought that a simpler approach, neglecting only the effects of far-field elastic non-linearities, might make use of the area changes of Burgers type circuits. Indeed, we have here shown that the change, from perfect lattice to final relaxed state, of the area of such a circuit is independent of the path taken in creating and relaxing the model. Allowance for outer-surface relaxation would be necessary to convert such circuit expansions into finite-body dilatations, but a more serious difficulty is the dependence on circuit size and position. The above results show that the circuit would have to be centered relative to the final dislocation line position and not relative to the coordinate origin, which is arbitrary. Even so no choice for circuit shape or position will guarantee correspondence between this method of estimating the formation volume and the more exact analysis. Finally, it is worth emphasizing that in the dislocation system investigated here, the elastic nonlinear term  $\delta A_{NL}$  is comparable to the core term, so that the full nonlinear analysis is in any case required, to give a realistic estimate of the total dilatation strength.

#### D. Core Field Representation by Line Force Dipoles

A final point of interest is the description of the core generated field in terms of a pair of orthogonal line force dipoles displaced from the dislocation line. The Flex-I calculations found such a representation, with the two dipoles at the same position, by a best fit to the relaxation displacements of atoms near the region I outer boundary. The present calculations allowed such a fit to be obtained directly from the dipole and quadrupole moments of the accumulated Green function source strengths, which totally characterize the displacement field outside the core. Again, however, it must be stressed that the result refers only to the relaxation field, and is dependent on the choice of initial positions. Table IV compares the Flex-I values with the present results using either Lagrange or Euler initial configurations. The rather poor agreement between the Flex-I and corresponding Flex-II results probably reflects the different fitting criteria: the Flex-I fit was near to the core, while the derivation from dipole and quadrupole moments represents a fit at "infinity".

#### IV. SUMMARY

A technique, Flex-II, has been described for applying flexible boundaries to an atomic model of a dislocation, crack tip or other line defect, so that compatibility is achieved between the core region and the outer region described in terms of continuum elastic solutions. The method has been found to be

superior to earlier flexible boundary schemes with respect to speed of computation. In the analysis of the core contributions to a dislocation strain field, nonlinear effects have been fully allowed for, without the necessity of employing a nonlinear elastic solution for the displacements. This analysis has enabled calculation of the overall dilatation of a finite body due to a dislocation, and earlier conflicting calculations of this quantity have been corrected and reconciled.

Acknowledgements

This research was supported in part by the U.S. Office of Naval Research and in part by the National Science Foundation, Grant DMR 74-21243.

References

1. J.E. Sinclair, J. Appl. Phys. 42, 5321 (1971).
2. P.C. Gehlen, J.P. Hirth, R.G. Hoagland and M.F. Kanninen, J. Appl. Phys. 43, 3921 (1972).
3. R.G. Hoagland, Ph.D. thesis, Ohio State University, Columbus, Ohio, June 1973.
4. R.G. Hoagland, J.P. Hirth and P.C. Gehlen, Phil. Mag. 34, 413 (1976).
5. M.P. Puls and C.H. Woo, Whiteshell Nucl. Res. Estab., Pinawa, Manitoba, Rept. AECL-5238 (1975).
6. J.E. Sinclair, Phil. Mag. 31, 647 (1975).
7. R.A. Johnson, Phys. Rev. 134, A1329 (1964).
8. A. Englert, H. Tompa and R. Bullough, in "Fundamental Aspects of Dislocation Theory", NBS Spec. Publ. 317, U.S. Govt Printing Office, 1970, p. 273.
9. Z.S. Basinski, M.S. Duesbery and R. Taylor, Phil. Mag. 21, 1201 (1970).
10. V. Vitek and M. Yamaguchi, J. Phys. F: Metal Phys. 3, 523 (1973).
11. R.J. Asaro, J.P. Hirth, D.M. Barnett and J. Lothe, Physica Stat. Sol. (b) 60, 261 (1973).
12. A.N. Stroh, Phil. Mag. 3, 625 (1958).
13. A.N. Stroh, J. Math. and Phys. 41, 77 (1962).
14. P.C. Gehlen, J. Appl. Phys. 41, 5165 (1970).
15. R. Fletcher and C.M. Reeves, Computer J. 7, 149 (1964).

16. J.E. Sinclair and R. Fletcher, *J. Phys. C.* 7, 864 (1974).
17. J.P. Hirth and J. Lothe, *J. Appl. Phys.* 44, 1029 (1973).
18. J.D. Eshelby, *Solid State Phys.* 3, 79 (1956), ed. Seitz and Turnbull.
19. J.R. Willis, *Int. J. Engng Sci.* 5, 171 (1967).
20. C. Teodosiu, V. Nicolae and H. Paven, *Physica Stat. Sol.* (a) 27, 191 (1975).
21. F. Granzer, V. Belzner, M. Bucher, P. Petrasch and C. Teodosiu, *J. Physique Colloq.* 34, C9-359 (1973).
22. P. Petrasch and V. Belzner, *J. Physique Colloq.* in press, 1976.
23. J.E. Sinclair and J.P. Hirth, *J. Phys. F: Metal Phys.* 5, 236 (1975).
24. J.P. Hirth, R.G. Hoagland and P.C. Gehlen, *Int. J. Solids Struct.* 10, 977 (1974).
25. P.C. Gehlen, G.T. Hahn and A.R. Rosenfield, *J. Appl. Phys.* 39, 5246 (1968).

Table I  
Atom Spacings in the Core Region for Various  
Simulation Methods

Method	Aniso-Tropy? <sup>a</sup>	Atoms in region I	Atom pair <sup>b</sup>			
			AB	DE	CF	BE
Rigid Boundary	no	780	2.3958	4.3839	4.2858	2.3978
Rigid Boundary	no	90	2.3828	4.2887	4.3452	2.3937
Flex-S	yes	200	2.3966	4.3907	4.2858	2.3981
Flex-I	no	340	2.3970	4.3925	4.2837	2.3979
Flex-II	no	236	2.3973	4.3942	4.2849	2.3979
Flex-II	yes	236	2.3968	4.3929	4.2850	2.3979

a) Isotropic models used Voigt average elastic constants

$$\mu = 8.6, \lambda = 12.1 (10^{11} \text{ dyn cm}^{-2})$$

b) See figure 2 for atom labels. Lengths in  $\text{\AA}$

Table II  
Area of Circuit Around Dislocation, Enclosing  $134\frac{1}{2}$  Atom Rows, with Initial Positions Generated as in Figure 3a-d

Relaxation by Flex-II with 152 atoms in region I; Areas, in units of  $b^2$ , may be compared with perfect lattice value 67.25. Burgers vector  $b = 2.86\text{\AA}$ .

Case (see Fig. 3)	Area in initial configuration	Area after relaxation	Change during relaxation
a	67.4257	67.6787	0.2529
b	67.2723	67.6776	0.4054
c	67.4262	67.6818	0.2555
d	67.2537	67.6695	0.4158

Table III  
Contributions to Total Volume of Formation of Dislocation

Two cases (see text) using Eulerian Volterra solution for initial positions.

Case	Fig. 3(d)	Fig. 3(d) with 0.1b added to $u_2$
$\alpha_1$	-0.0503	-0.0503
$\alpha_1 \ln(r_0/\text{\AA})$	0	-0.1
$M_{11}/\text{eV\AA}^{-1}$	6.876	5.884
$M_{22}/\text{eV\AA}^{-1}$	2.725	2.238
$\alpha_3$	0.6521	0.5517
$\alpha_4$	0.1204	0.1204
$r_1/\text{\AA}$	19.1	19.2
$\alpha_{\text{core}}$	0.3706	0.3696
$\alpha_{\text{NL}}$	0.0701	0.0701

Table IV  
Description of Relaxation Displacement Field in  
Terms of Line Force Dipoles

Dipole strengths are in  $eV\text{\AA}^{-1}$ , positions in  $\text{\AA}$ . All dipoles have coordinate  $x_1 = 0$ .

Case	$M_{11}$	$x_2$ position	$M_{22}$	$x_2$ position of $M_{22}$
Flex-I as fig. 3(a)	9.4	-5.2	2.8	-5.2
Flex-II as fig. 3(a)	5.0	-6.1	0.8	-7.7
Flex-II as fig. 3(d)	6.9	-2.5	2.7	-1.0

Figure Captions

Fig. 1 Concentric arrangement of regions for Flex-II model.

The Shape need not be circular.

Fig. 2 Relaxed configuration of the core of a [100] edge dislocation in bcc iron. Two (001) layers are distinguished.

Fig. 3 Four different methods of obtaining initial dislocated configuration from the Volterra solution. (a), (b) and (c) use Lagrangian coordinates, with the plane of discontinuity (a) on the positive  $x_2$  axis, with a half plane of atoms inserted; (b) on the  $x_1$  axis, so that slip is the formation process; (c) on the negative  $x_2$  axis, with a half plane of atoms removed. In (d), Eulerian coordinates are used, and the location of the plane of discontinuity is immaterial.